How dry was the Messinian Salinity Crisis?

- a molecular biogeochemical study of the Eraclea Minoa (Sicily) section, Italy -

Master Thesis within the master program Earth Sciences (Biogeology),

Eveline Mezger,

Utrecht University 2012

Supervised by Gert-Jan Reichart and Iuliana Vasiliev

Abstract

The Messinian Salinity Crisis (MSC; 5.96-5.33 Ma) is considered one of the most enigmatic episodes of paleo-oceanographic change during the Cenozoic era. Kilometres thick evaporites are deposited in the Mediterranean basin, during periods when the connections between the Atlantic Ocean and the Mediterranean were restricted. The development through time of this crisis is still under debate. Although it is generally accepted that the MSC was a dry period with higher evaporation than precipitation and runoff, how dry climate was and how saline the water, has not yet been quantified accurately. Samples from the Upper Evaporites (MSC stage 3; 5.50 - 5.33 Ma) were collected from the Eraclea Minoa section (Sicily), consisting of cyclic alternations of gypsum and marls. The main aim of this study is to reconstruct changes in the hydrological cycle during Upper Evaporite deposition. The hydrogen isotopic distribution is closely related to the hydrological cycle and build into organic molecules. This offers the opportunity to reconstruct past changes in the hydrological cycle and salinity using compound specific hydrogen isotopic analyses. The δD of terrestrial *n*-alkanes (C_{25} – C_{31}) mainly records the δD of precipitation, modified by site specific meteorologic conditions and evapotranspiration in leaves. The δD of long chain ketones, produced by haptophyte algae, mainly depends on the δD of the seawater, but also on salinity and to some degree growth rate. Both long chain *n*-alkanes with an odd over even predominance (higher plants), short chain marine *n*-C17 and long chain ketones were found, recording heavy (deuterium enriched) hydrogen isotopic values. The very heavy surface water values are in line with exceptional high rates of evaporation. The $U^{k'}_{37}$ values based on the same long chain ketones suggest overall relatively high SST (albeit at the maximum of the available calibration range) which, together with extremely dry conditions might have contributed to the extreme evaporation rates. Still, the presence of long chain ketones and absence of the C37:4 ketone in the Upper Evaporites suggests that connections between the Atlantic and Mediterranean, despite being reduced, were also open during stage 3 of the MSC. The reconstructed hydrogen isotopic composition of the precipitation is dependent on the fractionation factor used. The deuterium enriched precipitation values in a temperate (European) climate setting could be the result of the more heavy hydrogen isotopes from the seawater being reflected in local rain on the Mediterranean coast, albeit that admixing of marine organic matter contributed to the heavy values as well. However, the hydrogen isotopic composition of precipitation in a dry climate setting are comparable to present-day values and reconstructed salinities average around 65 g/l, which suggests a dilution of the Mediterranean surface water and a stratification of the water column. This stratification could explain the formation of gypsum deposits in brine circumstances in the lower water column and survival of open ocean haptophyte algal species in the upper water column. Overall, high SST appear to coincide with the deposition of marls and sandstones at the start of the cycle and massive gypsum in the upper part of the cycles. However, hydrogen isotopic values are most deuterium enriched in the massive gypsum deposits where most evaporation takes place during an insolation minimum, while the most depleted values occur in the marls at the start of the cycle coinciding with an insolation maximum and a high freshwater input. More measurements are needed to study these small scale changes in hydrogen isotopic values and their relation to climatic changes in detail.

Contents

1. Introduction 4
2. Background 6
2.1 Stratigraphic framework and geological history 6
2.2 Eraclea Minoa 6
2.3 The hydrological cycle and hydrogen isotopic composition of water 8
2.4 Biomarkers 8
2.4.1 *n*-Alkanes 9
2.4.2 Ketones 10
3. Methodology and techniques 11
3.1 Sampling strategy 11
3.2 Extraction techniques 11
3.3 Removal of elemental Sulphur 12
3.4 Fraction separations, Urea adduction and Methylation - Silylation 12
3.5 Identifications: GC, GC/MS, GCxGC-TOF(MS) 12
3.6 Compound specific hydrogen isotopic measurements 13
3.6 CPI, ACL and $U^{k'}_{37}$ 14
4. Results 15
4.1 Total lipid extract: biomarkers 15
4.2 *n*-Alkanes 15
4.3 Ketones 16
4.4 Hydrogen isotopes 17
4.5 Lithology versus results 18
5. Discussion 23
5.1 *n*-Alkanes 23
5.1.1 Identification 23
5.1.2 Hydrogen isotopes 23
5.2 Ketones 24
5.2.1 Identification 24
5.2.2 Hydrogen isotopes 25
5.3 Environmental reconstruction 25
5.3.1 Sea Surface Temperatures 25
5.3.2 Salinities 25
5.3.3 Overall changes Eraclea Minoa: a new hypothesis 27
5.3.4 Small scale changes (cycle 6) 28
6. Conclusions 30
7. Acknowledgements 30
References 31

1. Introduction

The Messinian Salinity Crisis (MSC; 5.96-5.33 Ma) is considered the most enigmatic episode of oceanic change during the Cenozoic era (1,2,3). Kilometres thick evaporates, trapping more than 5% of the world's oceanic salt, are deposited in the Mediterranean basin when the connections between the Atlantic and the Mediterranean were restricted (1,4). During precession maxima (insolation minima), evaporite deposition occurred because of the dry climate with higher evaporation than precipitation (1). In the late Miocene (~8 Ma), marine passages to the Atlantic were located in southern Spain and northern Morocco (Figure 1). Mechanisms for the closure of these passages and the isolation of the Mediterranean are under debate, including tectonic processes; a global sea level drop; or a combination of both factors (1,5,6,7). In the Late Miocene, an increase in volume of the Antarctic ice cap caused a worldwide lowering of the global sea level, which is inferred to have fluctuated by up to 30 meters during the deposition of the Lower Evaporites (5.96 – 5.55 Ma) (8,9,10). These fluctuations might have been the same during deposition of the Upper Evaporites (5.50 - 5.33 Ma), although oxygen isotopes also indicate a slightly warmer climate and a global sea level rise (10,11,12). Most theories about the MSC agree that the initiation of this crisis resulted from a complex combination of tectonic and glacio-eustatic processes, which progressively isolated the Mediterranean basin from the Atlantic Ocean. However, high-resolution stratigraphy and 'tuning' of the sedimentary cycle patterns suggest that the most prominent glacio-eustatic sea-level falls clearly post date the onset of evaporite deposition, while the timing of plate tectonic processes coincides much better with the sedimentary cycle patterns (1). According to Duggen et al. (2003), a westward roll back of subducted Tethys ocean lithosphere combined with an associated asthenospheric upwelling produced the necessary uplift along the African and Iberian continental margins to close the marine gateways (7). At the start of the Pliocene, a catastrophic flooding due to the opening of the Strait of Gibraltar led to the end of the MSC (Figure 1) (7).

Figure 1 Modified NASA photograph of the westernmost Mediterranean to show Atlantic–Mediterranean marine gateways in southern Spain and northwestern Africa about 8 Ma, based on the distribution of reef complexes and marine sediments (which now outcrop several hundred meters above sea level) (7,13).

Although it is generally accepted that the MSC was a dry period with higher evaporation than precipitation and runoff, how dry climate was and how saline the water has not yet been quantified accurately. The Upper Evaporites were studied to answer this question. In contrast to the evaporite dominated Lower Evaporites, the Upper Evaporites are dominated by non-evaporitic deposits intercalated with gypsum (12). During deposition

of the Upper Evaporites, it is assumed that isolation from the Atlantic Ocean has been established (14). Most studies agree that the lowest Mediterranean water levels were reached during deposition of the Upper Evaporites in shallow brine pools, more than a thousand meters below the global sea level (2,11). Environmental conditions remain controversial: sedimentary observations suggest a highly fluctuating Mediterranean water level during Upper Evaporite deposition, while paleontological and geochemical data indicate that oceanic influxes continued to enter the Mediterranean, during which the freshwater contribution increased significantly upwards resulting in a brackish water column of the Lago Mare facies (2,11,15). The most significant Messinian basins of Italy are the Northern Apennines foreland basin, Tertiary Piedmont basin, the Sicilian-Maghrebian foreland basin, the Tuscany basins and the Crotone basin. Amongst these basins and also at Mediterranean scale, the Apennine and Sicily marginal basins are the largest ones, containing over 1000 meters of Messinian succession (14). In this study, samples from the Upper Evaporites (MSC stage 3; 5.50 - 5.33 Ma) were collected from the Eraclea Minoa section (Sicily), consisting of cyclic alternations of gypsum and marls (Lago Mare). The main aim of this study is to reconstruct changes in the hydrological cycle and salinity during Upper Evaporite deposition in both high (in-cycle changes) and low resolution. The hydrogen isotopic distribution is closely related to the hydrological cycle and build into organic molecules, since photosynthetic organisms use water as the main hydrogen source by photosynthesis ($CO_2 + H_2O \rightarrow CH_2O + O_2$) (16,17). This offers the opportunity to reconstruct past changes in the hydrological cycle using compound specific hydrogen isotope analysis. Still, this approach critically relies on the availability, preservation and identification of biomarkers suited for such reconstruction. In this study, compound-specific hydrogen isotopic measurements on both terrestrial (*n*-C25-C31) and aqueous biomarkers (*n*-C17 and long chain ketones) were performed to reconstruct paleohumidity and salinity during deposition of the Upper Evaporites. Furthermore, sea surface temperatures (SST) were calculated and the relationship between lithology and the calculated parameters were studied in both small and large scales.

2. Background

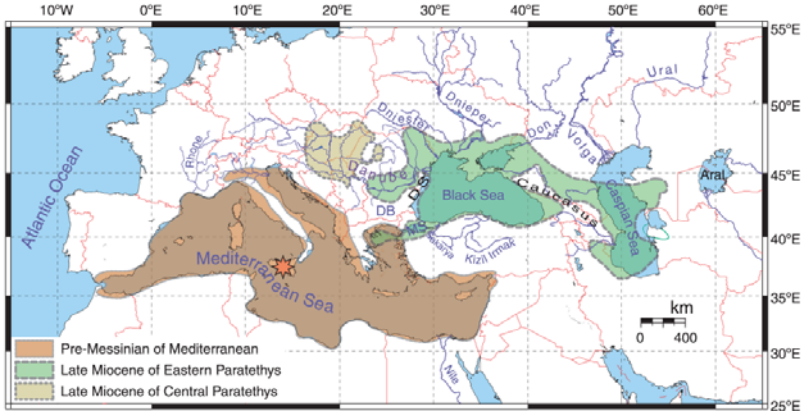

Figure 2 Location of the Eraclea Minoa section in Sicily, Italy (modified after Vasiliev, in press).

2.1 Stratigraphic framework and geological history

The Messinian sequence as described from Sicily (~7.24 – 5.33 Ma) starts with alternations of open marine marls and sapropels succeeded by diatoms, followed by the 'Lower Evaporites' including gypsum, evaporitic limestone, marls and halite and after an erosional surface into the 'Upper Evaporites' (marls, gypsum) and brackish to freshwater deposits of the 'Lago Mare' facies (1,2,4). This succession is known from the largest basin of Sicily: the Caltanissetta basin (Figure 2). The Caltanissetta basin is the main depozone of the Maghrebian-Sicilian foreland basin system, of which the evolution is only related to that of the Apennines foredeep basin. The succession can be divided into the previously mentioned units (respectively the Lower and Upper Evaporites), separated by the Messinian Erosional Surface (MES) (14). This erosional surface is found in marginal settings and interpreted as a sea level drop related feature, leading to fluvial rejuvenation, and/or local tectonic activity (1). The lower unit contains the Lower Gypsum of the Gessi di Cattolica Formation and the Calcare di Base Formation, its lateral equivalent at basin margins consisting of several types of carbonate rocks. Dependant on the model, a halite unit either overlies the Lower Gypsum and Calcare di Base through a horizon of gypsum turbidites or lateral transitions between these lithologies occur (12,14,18,19). The upper part of the succession consists of the Upper Gypsum (Gessi di Pasquasia Formation), containing cyclic alternations of primary gypsum (laminar gypsum and selenite) and brackish to continental marls, recording the last phase of the MSC (Lago Mare). The marine Zanclean Trubi Formation overlies the Upper Evaporites (14).

2.2 Eraclea Minoa

Samples of the Upper Evaporites (5.50 – 5.33 Ma) are collected from the Eraclea Minoa section (Sicily), consisting of 8 cycles (Figures 2 and 3). In general, most cycles start with an alternation of marl and sandstone beds (facies A), succeeded by clastic gypsum beds (gypsarenite, gypsrudite and graded marl beds) and primary evaporitic laminar gypsum beds (gypsum cumulate) (facies B), and end with massive selenite (selenite crust, massive selenite beds separated by thin marl layers, domed selenites and reworked selenites on top of the domes, facies C) (20). The section is preceded by Resedimented Lower Gypsum (RLG), consisting of a gypsum turbidite megabed with Primary Lower Gypsum blocks, and gypsum cumulate. Cycle 1 only consists of banded selenites, succeeded by a partially covered area of approximately 43 meter belonging to cycle 2. Cycle 2 contains thin marl layers, selenite crust and massive selenite. After a partially covered area, cycle 3 consists of marls, followed by a selenite crust and massive selenites. Cycles 4, 5, the first part of cycle 6 and 7 have the 'basic' cycle pattern. Cycle 6 consists of three parts, of which the last two sub-cycles mainly consist of marls, thin bedded sandstones and sandstone bars (only the marls are sampled for organic geochemical purposes). Cycle 6^2 and cycle 8 also contain melanopsis and ostracod fossils. Cycle 8 consists of marls and the 'Arenazzolo' sandstone beds. The Pliocene samples only contain marls. An overview of the section and the processed samples is given in Figure 3.

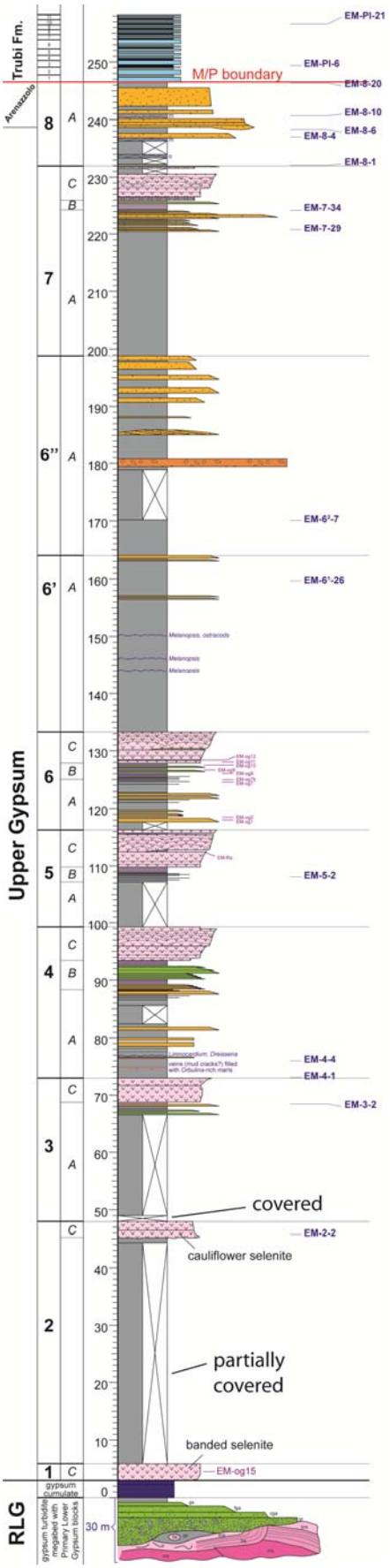

Figure 3 Schematic lithological column of the Eraclea Minoa section, including the processed samples of this study (modified after Manzi et al., (2009) (20)).

2.3 The hydrological cycle and hydrogen isotopic composition of water

Hydrogen isotopes, being interrelated to the hydrological cycle and build-in organic molecules offer the opportunity to reconstruct past changes in the hydrological cycle. Hydrogen has the largest relative mass difference between its stable isotopes, ^{1}H and ^{2}H (D), and, as a consequence, the largest natural variation in stable isotope ratios (16). The ratio between these isotopes vary in response to climatic and environmental change, which makes it a suitable proxy for hydrographic changes in response to evaporation and relative humidity (21). Since photosynthetic organisms use water as the main hydrogen source by photosynthesis (CO_2 + H_2O -> CH_2O +O_2), the deuterium concentration in the environmental water is reflected by the deuterium composition of the organism (16,17,22). To reconstruct the hydrogen isotopic composition of environmental water, the influence of the environment and physiology need to be known (Figure 4). Different organisms have different water sources, e.g. the water source of terrestrial plants is soil water, which is directly related to precipitation. The δD of precipitation varies over time and space, caused by several environmental factors: the continental effect, the amount effect and the temperature effect (Figure 4) (23). Further inland, δD values of precipitation decrease due to preferential loss of deuterium in a moving air mass. Furthermore, the isotopic composition of precipitation is more depleted in δD at higher precipitation rates and more fractionation takes place when temperatures are low (22,23). Summarised, the stable water isotopes in precipitation reflect the source region, water loss during transport, local temperature and the contribution of local water and mixing of air masses (21,24,25). Soil water can be altered by surface evaporation and deuterium enrichment by exchange with the atmosphere in the upper soil horizons. However, plants in these arid regions are adapted to these circumstances and take up water from deeper soil horizons, not influenced by surface evaporation. Therefore, in general the plant-source water δD values follow those of precipitation at large spatial scales (22,26). Aquatic organisms (e.g. algae and aquatic plants) use precipitation, accumulated in lakes, rivers and bogs as their main hydrogen source (22). The hydrogen isotopic composition of seawater mainly depends on the intensity of evaporation and influx of freshwater by rivers (27). Especially in arid regions, evaporation could locally exceed precipitation and the residual water becomes increasingly enriched in deuterium (22).

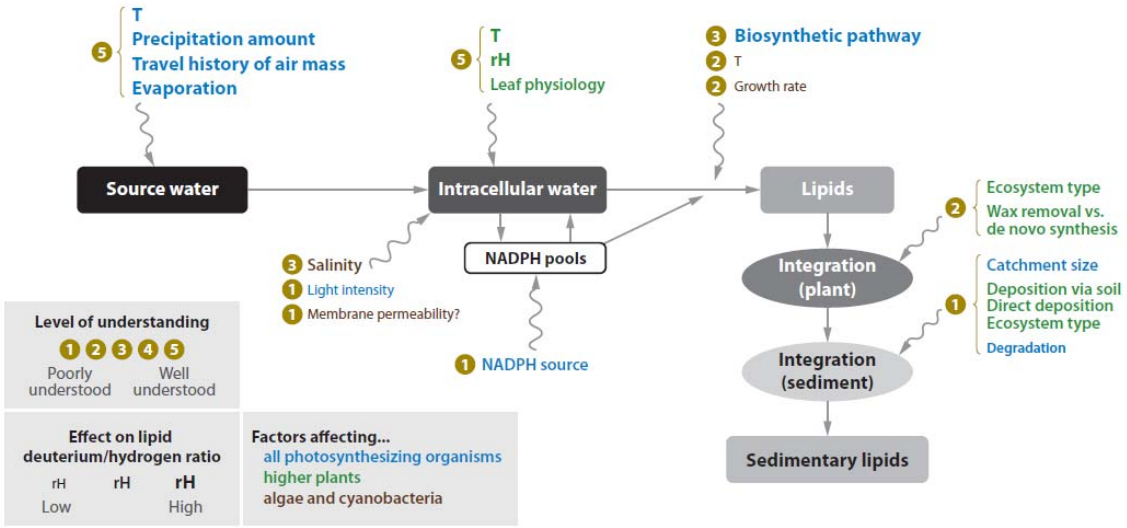

Figure 4 Overview of all processes that affect the δD of lipid biomarkers (e.g. *n*-alkanes and ketones), produced by phototrophic organisms. With T: temperature and rH: relative humidity (22).

2.4 Biomarkers

Since water is the source for all photosynthetic products, the hydrogen isotopic composition of lipids produced by aquatic and terrestrial organisms can be related to the δD of their source water. By the use of compound-specific hydrogen isotopic ratios of sedimentary biomarkers, paleohydrology has been

reconstructed over different geological timescales. Several lipids that can be used for this purpose are fatty acids, hopanols, ketones, sterols and wax esters. These are present in the membranes of algae, bacteria and higher plants and could be specific for certain species. Furthermore, higher terrestrial plant leaves with a cuticular wax layer contain long chain *n*-alkanes, *n*-alcohols, *n*-alkanoic acids and triterpenoid compounds (22,28). The main advantage of lipids is the covalent bond between hydrogen and carbon atoms, which cannot be exchanged easily at temperatures below 100˚Celsius (18,22). However, during transport from the source environment to the place where biosynthesis takes place, the isotopic composition of the water could change substantially (22). Most organic molecules are depleted in deuterium compared to the environmental water due to (biosynthetic) fractionation (Figures 4 and 5) (22). Several environmental factors could also affect the hydrogen isotopic composition of lipids, including light intensity, growth rate, growth stage, salinity and temperature (Figure 4) (27,22). Furthermore, the δD also depends on the biosynthetic pathway (e.g. the acetogenic pathway for *n*-alkanes), secondary hydrogen exchange reactions, hydrogenations and dehydrogenations (22). In this study, both *n*-alkanes and ketones are discussed and used to reconstruct changes in the hydrological cycle.

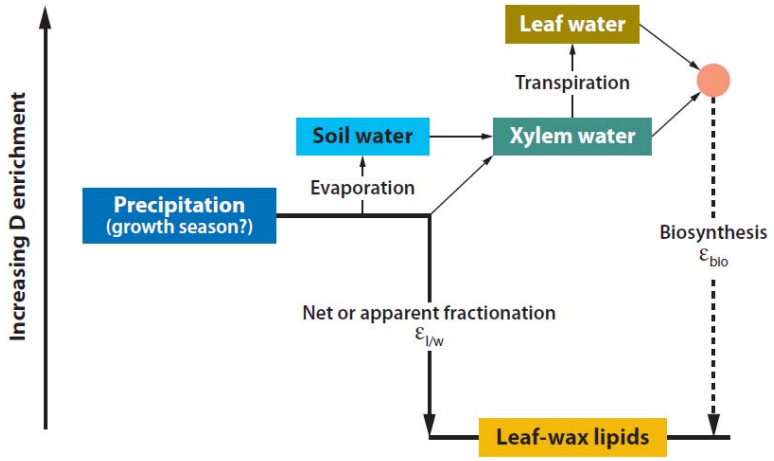

Figure 5 Fractionations between the source water (precipitation) and terrestrial *n*-alkanes in a conceptual diagram with $\varepsilon_{l/w}$: isotopic fractionation between lipids and source water, ε_{bio}: biosynthetic fractionation and the red dot represents a (hypothetical) biosynthetic water pool (modified by Sachse et al. (2012) after Sachse et al. (2006) and Smith and Freeman (2006) (22,29,30)).

2.4.1 *n*-Alkanes

N-alkanes are very abundant in sediments from all geological periods, easy to extract and purify and contain non-exchangeable hydrogen atoms because they are carbon bound (29,31). In general, short chain *n*-alkanes with a carbon number of 17 or 19 are produced by algae, *n*-alkanes with a carbon number of 21 and 23 are produced by submerged aquatic plants or *sphagnum* species and *n*-alkanes with an (odd) carbon number between 25 and 31 are derived from terrestrial higher plants (29,32,28,33). In previous studies, the hydrogen isotopic composition of terrestrial *n*-alkanes, as well as other lipids derived from terrestrial plants, were measured in several lake-surface sediments and showed a strong linear relation with the δD of the mean annual precipitation with a relatively constant offset (e.g. 22,34). Variations in the δD of *n*-alkanes are not only caused by changes in the hydrogen isotopic composition of the precipitation itself, but are also influenced by numerous fractionation steps that contribute to the overall net fractionation, of which biosynthetic fractionation, leaf-water and soil-water evapotranspiration are the most important sources (Figures 4 and 5, 22). The δD of terrestrial *n*-alkanes (C25–C31) mainly records the δD of precipitation, modified by site specific meteorological conditions (e.g. evapotranspiration in leaves and relative humidity) and isotope enrichment due to plant anatomy (Figure 5, 29). The relative contribution of soil-water and leaf-water evapotranspiration to the overall fractionation is poorly understood, but the importance of these processes is shown in the following

examples: the deuterium enrichment in terrestrial leaf-wax *n*-alkanes relative to aquatic *n*-alkanes; the deuterium enrichment in lake sediments in drier regions compared with temperate regions; and in living terrestrial plant *n*-alkanes in arid regions compared with those in wetter sites (22,34,35,36). Transpiration (water loss from the leaf) results in a deuterium enrichment of the leaf water, since lighter water isotopes evaporate and diffuse in air faster than heavier isotopes (22). Based on global data of the fractionations between the *n*-C29 and mean annual precipitation, a trend to less negative δD values is observed at locations with evapotranspiration <1,000 mm per year and a relative humidity of <0.7 (22,32,36). Other factors that contribute to the hydrogen isotopic composition of *n*-alkanes, which are not all well understood, are rooting depth, light intensity, life form and the photosynthetic pathway (22). Based on a sampling study in recent lakes on a N-S European transect, the biosynthetic fractionation between the source water and the *n*-alkanes is considered to be constant around a mean of -157‰ for both aquatic and terrestrial *n*-alkanes (29,37). For a modern European climate, a fractionation (respectively enrichment factor ε) of -130‰ between the δD of the terrestrial *n*-alkanes and the δD of the precipitation was found (37). Desert environments have a fractionation (ε) of -94‰, which is one of the smallest net fractionations recorded due to high leaf water deuterium enrichment in an arid environment (32). According to a lake sampling study by Sachse et al. (2004), terrestrial *n*-alkanes are enriched in deuterium by 10 to 60‰ compared to aquatic *n*-alkanes due to leaf evaporation processes (29,37). In this study sedimentary *n*-alkane accumulations were used for hydrological reconstructions, which include plant inputs over different time and from different spatial scales. This means that the hydrogen isotopic composition of the *n*-alkanes cannot be attributed to individual species, is biased toward the most important plant sources and less variability in sedimentary deposits compared to modern environments can be found (22).

2.4.2 Ketones

Long chain ketones are a good tool to reconstruct the hydrogen isotopic composition of the surface water since these possess covalently bound hydrogen atoms, which are not likely to be exchanged during diagenesis (18,27). Alkenones are a species-specific biomarker, unique to a small number of haptophyte algae within the order Isochrysidales, and assumed to be produced predominantly by *Emilianiania huxleyi* in marine sediments younger than 280 ky (13,38,39). Nowadays, the cosmopolitan coccolithophorid *Emiliania huxleyi* is an abundant species in coastal areas and the open ocean and the main producer of C37-C39 methyl and ethyl ketones (13). Other producers are *Gephyrocapsa oceanica* and members of the class *Prymnesiophycaea* (21,41). However, comparisons between laboratory and field experiments showed that the contribution in sediment cores of members of the class *Prymnesiophycaea* are of minor importance (40). Based on a culturing study, in which two species of haptophyte algae were cultured (*Emiliania huxleyi and Gephyrocapsa oceanica*) at different temperatures; salinities; and δD of the water, the δD of long-chain alkenones mainly depends on the δD of the seawater, but also on salinity and to some degree growth rate (27). The isotopic fractionation between the alkenones and the source water showed a decrease of 3-4‰ per salinity unit increase, while the δD of the culturing water itself only changed 1.7‰ per salinity unit (20). Several hypothesis for this mechanism are: lower growth rates at higher salinities, which could decrease the fractionation between the alkenones and water; deuterium enrichment of intracellular water through restricted exchange with extracellular water at high salinities; or increased osmolite production, which would preferentially remove the lighter hydrogen isotopes from the water in the cell (20,42,43). However, this mechanism is not resolved yet. In a culturing study with *Emilianiania huxleyi* and different stable hydrogen isotopic compositions of the culture medium by Paul (2002), the per mil enrichment factor (ε) between the δD of the C_{37} ketones and the culture media was relatively constant at ~-232‰ (44). In a more recent study, a similar fractionation (ε) of ~-225‰ was found for the C_{37} ketones and a fractionation of ~-233‰ for the C_{38} ketones, with fractionation factors of the slope of the regression (α) of 0.732 and 0.745 (13).

3. Methodology and techniques

3.1 Sampling strategy

The Upper Evaporites (5.50 - 5.33 Ma) of the Eraclea Minoa section in Sicily (Italy) were sampled, representing a marginal setting during the MSC. These samples were numbered according to their cycle number (up to 8), but also the location in a cycle. Samples were taken through time in a high resolution and as much facies as possible were sampled. Salt (halite) samples of the upper part of the Lower Evaporites were recovered from the Real Monte salt mine, Sicily. Samples were taken with geochemical bags, to avoid contamination of plastics (phthalates).

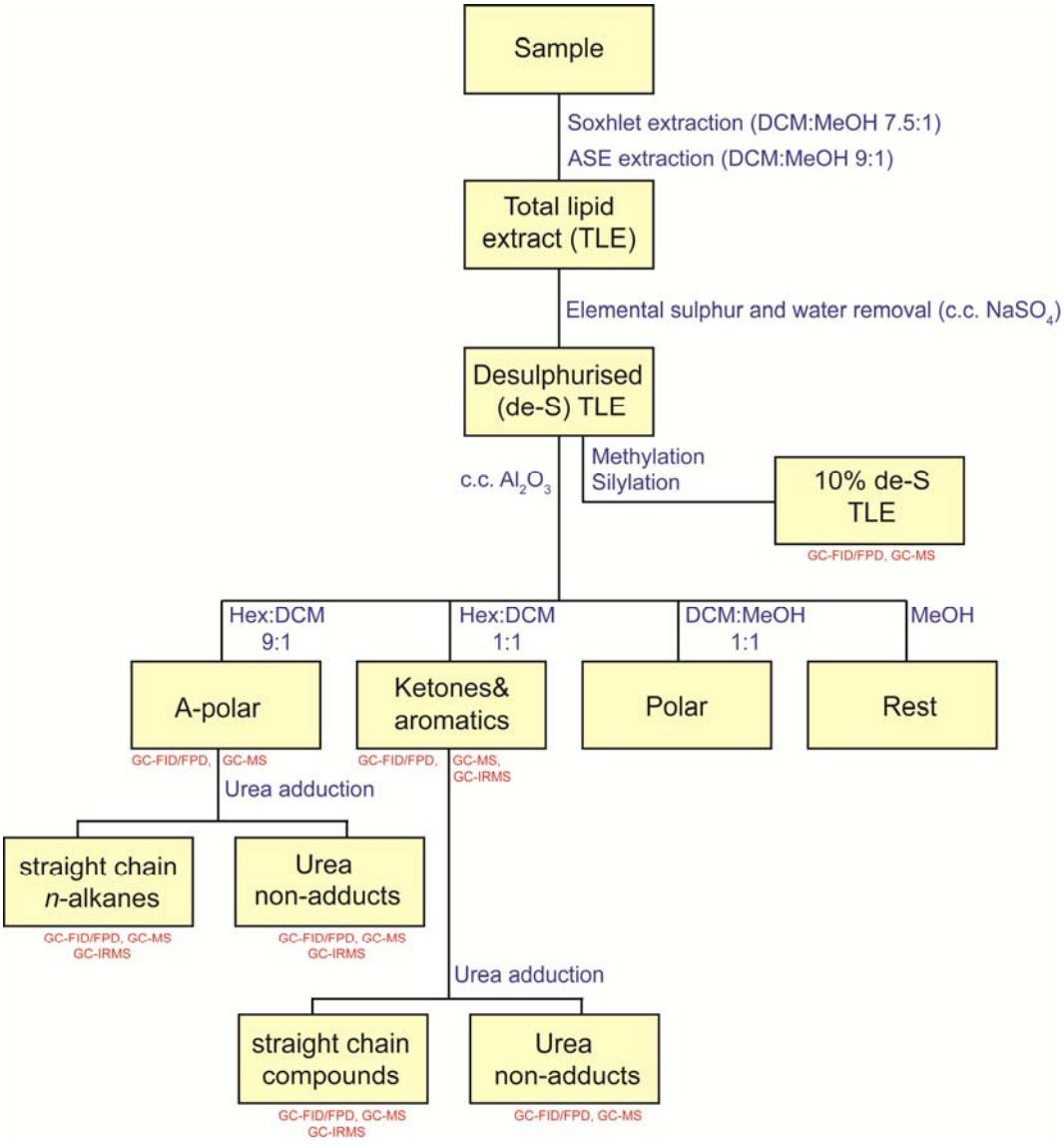

Figure 6 Flow diagram of the methods used, with the processes in blue, the measurement type in red and the obtained fractions in black.

3.2 Extraction techniques

An overview of the methods used is shown in Figure 6. Soxhlet and Accelerated Solvent Extraction (ASE, Dionex 200) were used for extraction of the organic compounds. Between 40 and 60 grams of fresh sedimentary rock of each sample was powdered and extracted for at least 24 hours at 80˚C with Soxhlet extraction, using a dichloromethane (DCM) – methanol (MeOH) (7.5:1, v/v) solution in a 250 ml round bottom

flask. The filters were cleaned before use. For the ASE extraction, approximately 20 grams of rock sample was powdered and a DCM - MeOH (9:1, v/v) solution was used. The smallest cells of the ASE were selected and the sample was mixed with diatomaceous earth to let the solvent seep through more easily. After extraction, the extracts were rotary-evaporated to near dryness and transferred to small vials with DCM. Subsequently, the DCM was removed under the nitrogen blower. If necessary, the Total Lipid Extracts (TLE) were rinsed over a (anhydrous) NA_2SO_4 column to remove molecular water.

3.3 Removal of elemental Sulphur

Elemental sulfur was removed with copper flakes, which were activated by the addition of 2M HCL and rinsed with bidistilled water until the pH of the water was neutral. A small stirring bar, a small volume of DCM and the copper turnings were added to the samples, which were stirred overnight. This procedure was repeated until the formation of copper sulfide (CuS) ended and no elemental sulfur was left. The de-sulphurized TLE was rinsed over a small pipette filled with Na_2SO_4 to remove the CuS and eventual molecular water.

3.4 Fraction separations, Urea adduction and Methylation - Silylation

The total lipid extract (TLE) was separated into the a-polar, alkenone, polar and rest fractions using small column chromatography with aluminum oxide (Al_2O_3) as a stationary phase. The Al_2O_3 was activated for approximately 2 hours at 150˚C. The column was rinsed with four column volumes (a column volume is respectively 1µl) of a Hexane: DCM solution (9:1, v/v) to elute the a-polar fraction, three column volumes of Hexane: DCM (1:1, v/v) to elute the alkenone fraction, three column volumes of DCM: MeOH (1:1, v/v) to elute the polar fraction and three column volumes of MeOH to elute the rest (most polar fraction). Straight chain *n*-alkanes were separated from branched the and/or cyclic hydrocarbons in the a-polar fraction by the urea-adduction method. The dry a-polar fraction was dissolved in 200 µl saturated urea solution in methanol (~10%) and subsequently, 200 µl acetone and 200 µl hexane were added. The samples were frozen and dried under the nitrogen blower, during which urea crystals were formed that capture the n-alkanes. The branched and cyclic hydrocarbons were removed by washing the sample with three volumes of hexane (the Urea non-adducted part). The urea crystals were dissolved in 500 µl bidistilled water and 500 µl ethyl acetate (EtAc). After the addition of hexane, the straight chain compound containing hexane layer was pipetted off (the Urea adducted part). This process was repeated three times.

Approximately 10% of the TLE was kept aside for other purposes, e.g. analysis of the total lipid composition, repetition of the separation process and quantifications. In order to analyze functional compounds of the sample, the TLE was measured on the Gas Chromatographer (GC) flame ionization detector (FID) and FPD (sulfur detector) and the Gas Chromatographer-Mass Spectrometer (GC/MS) after the methylation and silylation process. The methylation process was performed by the use of diazomethane and cleaned over a small silicagel column with Ethyl Acetate (EtAc). Silylation was performed with the addition of 30µl pyridine and 25µl BSTFA, after which it was stored in the oven at 60˚C for ~20 minutes to let it react. Subsequently, the sample was diluted in EtAc (20-100 µl) and measured on the GC-FID/FPD and GC/MS.

In order to quantify the *n*-alkanes and long chain ketones, an internal standard was added to the TLE of a few samples. This internal standard consists of squalane in a 50.2 µg/mL concentration, of which 20 µL (1.004 g squalane) was added to approximately 10% of the TLE. Quantities were determined by integration of the peaks in the gas chromatogram and comparing this area to the peak of the standard with a known amount.

3.5 Identifications: GC, GC/MS, GCxGC-TOF(MS)

The molecular composition of the obtained fractions was analyzed by gas chromatography (GC), gas chromatography-mass spectrometry (GC-MS, Thermo-Finnigan Trace DSQ) and comprehensive two

dimensional gas chromatography-time of flight (TOF)- mass spectrometry (GCxGC-TOF(MS)). The a-polar and alkenone fractions were dissolved in hexane and the silylated polar fractions in ethyl acetate. The *n*-alkanes and alkenones were identified using mass spectra, including molecular ion mass and retention times. Furthermore, the molecular composition of the alkenones was also studied by comprehensive two dimensional gas chromatography – time of flight – mass spectrometry with a reversed column set-up (GCxGC-TOF(MS), Agilent 7890, JEOL AccuTOF, ZOEX I) on the alkenone fraction of sample EM-6^2-7 (159.5 m stratigraphic level, 5.380 Ma). The sample was injected at 250˚C with Helium as a carrier gas at a constant pressure of 600 kPa. First-dimension separation (the polar column) was performed using a DB-17ms phase (Agilent, 50% phenyl - 50% methyl polysiloxane, 10m, 0.25mmID, 0.25um Df), of which the oven was held at 100°C for one minute, then raised from 100 to 250°C with 10°C min^{-1} and then raised from 250°C to 310°C with 1°C min^{-1} and held at 310°C for 20 minutes. The second dimension separation (the a-polar column) was performed using a DB-1ms phase (Agilent, 100% methyl polysiloxane, 2m, 0.10mmID, 0.10um Df). The second dimension oven was held at 130°C for one minute, after which it was raised from 130 to 280°C with 10°C min^{-1} and from 280°C to 340°C with 1°C min^{-1} and held at 340°C for 20 minutes. The interface temperature was 270°C. The modulator was a ZOEX-system, with a modulation period of 10s. The hot pulse had a duration of 0.4 seconds and a temperature offset of +50˚C compared to the primary oven temperature.

3.6 Compound specific hydrogen isotopic measurements

Compound specific hydrogen isotopes were measured on the gas chromatography- isotope ratio monitoring– mass spectrometer (GC-IRMS). The urea adducted a-polar or alkenone sample, dissolved in hexane, were injected on a HP 6890N Gas Chromatograph at 70˚C coupled to a Thermo-Finnigan DELTA^{plus}XL Isotope Ratio Mass Spectrometer at the Molecular Biogeochemistry laboratory of the Earth Sciences department, Utrecht University, using high temperature conversion. The oven is programmed to increase from 70˚C during injection to 130˚C at a speed of 20˚C per minute. Thereafter, the column was heated to and kept constant for 10 minutes at 320˚C with a speed of 5˚C per minute. A constant flow of 1.5 ml per minute of Helium was used as and a film thickness of the CP-Sil 5 column was 0.4µm. The H_3^+ factors were determined daily and varied between 5 and 6.5. H_2 gas with known isotopic composition was used as a reference. A mixture of C_{16}-C_{32} *n*-alkanes with a known isotopic composition (obtained from Dr. Arndt Schimmelmann, Indiana University) was used to monitor the performance of the system. Analysis were done, if possible, at least in duplicate. A squalane standard was co-injected with every sample with a hydrogen isotopic composition of approximately -171±3‰ (16).

For the fractionation of a single component (e.g. hydrogen), the following formula applies (45):

$$\partial_p = \propto \partial_s + \varepsilon \quad \text{or} \quad \partial_p = \propto \partial_s + (\alpha - 1) * 1000 \qquad \text{(a)}$$

In which δ_p represents the δD of the product, δ_s represents the δD of the source, α is fractionation factor from the slope of the regression and ε = α - 1 is the fractionation factor from the intercept of the regression and also called the per mil enrichment factor, assuming that per mil units imply a factor of 10^3 (13,45). For oxygen and carbon isotopes, α varies around 1 and the formula changes into: $\partial_p = \partial_s + \varepsilon$. However, such approximations are inappropriate for hydrogen isotopes, because of the very large fractionations in many biological systems that affect the hydrogen isotopic composition. The δD of plant lipids and environmental water are expected to be related through this equation, because water is the source of all hydrogen in plants. From several sampling studies of plant lipids from lakes, a significant disagreement between the implied fractionations of the intercept (ε) and slope (α) of each of the regressions was found which implies that the relationship is not as simple as assumed (45,46,47,48). However, the derived equations (as with any statistically significant correlation) can still be used to predict hydrogen isotopic compositions for environmental water, but should not be interpreted a single fractionation step between water and lipid (45). This means that a single fractionation factor in this formula represents the net effect of all biosynthetic processes. For *n*-alkanes, fractionation factor ε can be described as (37):

$$\varepsilon_{alkane/water} = 1000 * (\frac{\partial D_{alkane}+1000}{\partial D_{source\ water}+1000} - 1) \quad \text{(b)}$$

For the δD of the source water rewritten into:

$$\partial D_{source\ water} = \frac{1000*(\partial D_{alkane} - \varepsilon_{alkane/water})}{\varepsilon_{alkane/water}+1000} \quad \text{(c)}$$

Of which a value of -130‰ represents the $\varepsilon_{alkane/water}$ for terrestrial *n*-alkanes in a temperate (European) climate, -94‰ represents the $\varepsilon_{alkane/water}$ in desert regions and -157‰ represents the $\varepsilon_{alkane/water}$ for aquatic *n*-alkanes, which only includes the biosynthetic fractionation (29,32,37). Again, the fractionation factor does not represent a single fractionation between the source water and the (in this case) *n*-alkanes or ketones, but the net effect of all fractionations during biosynthetic processes. For ketones, formula 1 can be rewritten into (27,45):

$$\partial D_{alkenones} = \propto \partial D_{water} + (\propto -1) * 1000 \quad \text{(d)}$$

Where

$$\propto = \frac{(\frac{D}{H})_{alkenones}}{(\frac{D}{H})_{water}} \quad \text{and} \quad \alpha_{alkenones-H2O} = \frac{1000 + \partial D_{alkenones}}{1000 + \partial D_{water}} \quad \text{(e)}$$

The per mil enrichment factors (ε = (α - 1) * 1000) obtained from a culturing study for the C37 and C38 ketones are respectively -225‰ and -233‰, with fractionation factors of the slope of the regression (α) of 0.732 and 0.745 (13).

3.6 CPI, ACL and $U^{k'}_{37}$

The terrestrial contribution and eventual changes in the composition of the vegetation of the long chain *n*-alkanes were determined by calculating the carbon preference index (CPI) and the average chain length (ACL) by integration of the peak areas in the gas chromatogram. The following formulas were used to calculate these values:

$$\mathrm{ACL} = \frac{25*A25+27*A27+29*A29+31*A31+33*A33}{A25+A27+A29+A31+A33} \quad \text{(f)}$$

$$\mathrm{CPI} = \frac{\mathrm{A25+A27+A29+A31+A33}}{\mathrm{A24+A26+A28+A30+A32}} + \frac{\mathrm{A25+A27+A29+A31+A33}}{\mathrm{A26+A28+A30+A32+A34}} * 0.5 \quad \text{(g)}$$

Furthermore, the alkenone unsaturation index ($U^{k\prime}_{37}$) was calculated, monitoring the ratio between the di- and tri-unsaturated alkenones (17). These alkenones are produced nowadays by haptophyte algae (18). The peak areas were determined by GC analysis.

$$\mathrm{U}^{\mathrm{k}\prime}_{37} = \frac{C37{:}2}{C37{:}2+C37{:}3} \quad \text{(h)}$$

4. Results

An overview of all results of the Eraclea Minoa section, including the CPI and ACL values of the *n*-alkanes and compound specific hydrogen isotopic measurements is given in Figure 10. Figure 11 shows these measurements on a smaller scale (cycle 6), in order to look at the homogeneity of the results within a cycle. The compound specific hydrogen isotopic measurements of both the *n*-alkanes as well as the ketones, stratigraphic levels of the samples and lithologies are given in Tables 1 and 2. Ages of the samples are determined with the assumption of a constant sedimentation rate within a cycle and the duration of a cycle is assumed to be 21.7 kyr (averaged duration of a precession cycle).

4.1 Total lipid extract: biomarkers

The results of a total lipid extract (TLE) measurement from the Eraclea Minoa section are shown in Figure 7. Both ketones (a,b,c) and *n*-alkanes (e-m) are dominant throughout the spectrum and also hopanes and steranes (o,p,q) are found. Based on these results, hydrogen isotopic measurements were applied on both ketones and *n*-alkanes. The first part of the spectrum is not discussed into detail because of the contamination (r,s, Figure 7).

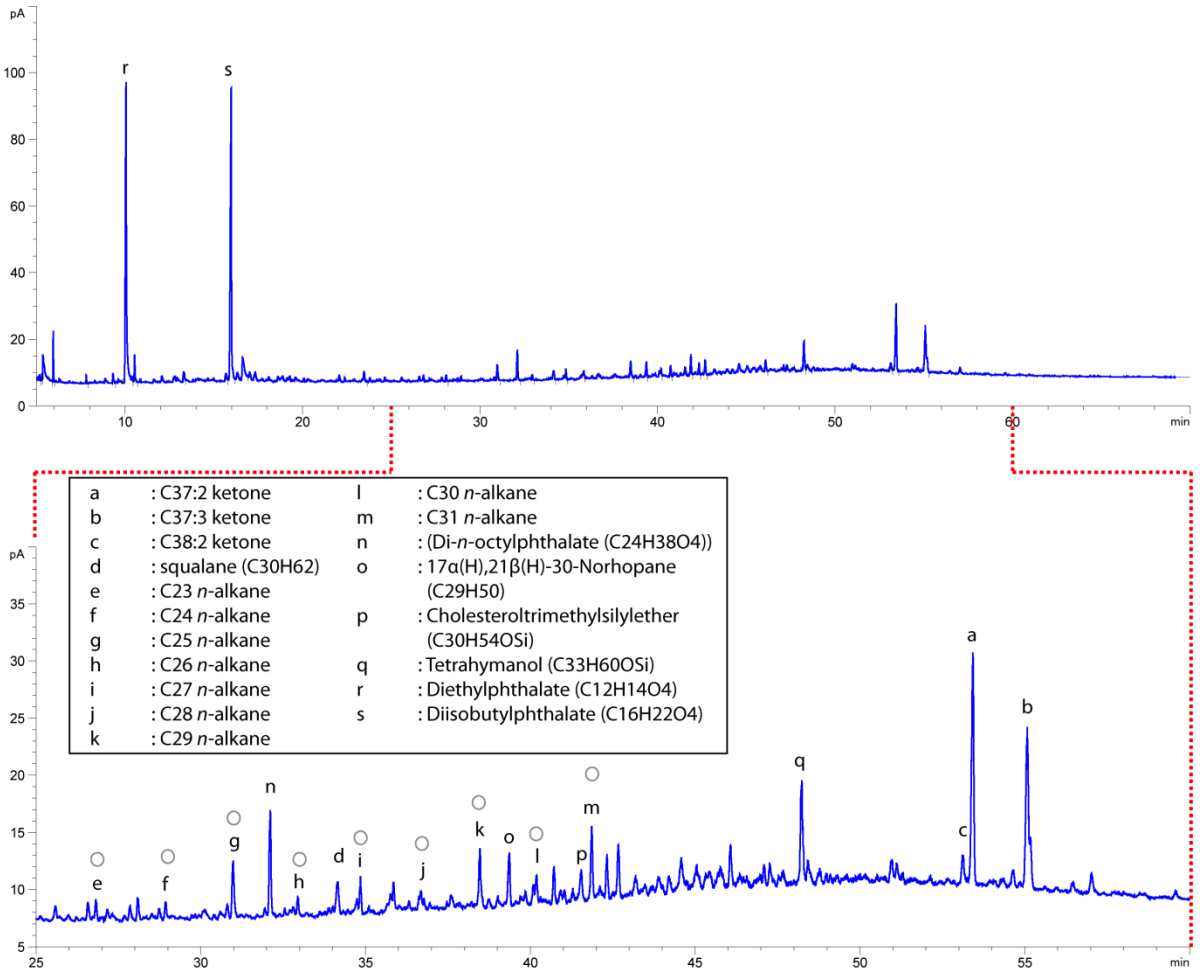

Figure 7 Example of a Methylated-Silylated total lipid extract (TLE) from Eraclea Minoa. Ketones (a,b,c) and *n*-alkanes (e-m, open circles) are present, as well as hopane and sterane structures (o,p,q).

4.2 *n*-Alkanes

Excellently preserved short (C16-C23) and long chain *n*-alkanes (C25–C33) are found throughout the entire section (Figure 8). Quantities vary between 0.032 and 0.058 µg per gram of sediment (µg/g) for the *n*-

C23, between 0.022 and 0.046 µg/g for the *n*-C25, 0.024 and 0.053 µg/g for *n*-C27, for the *n*-C29 between 0.033 and 0.098 µg/g, between 0.033 and 0.130 µg/g for *n*-C31 and between 0.053 and 0.067 µg/g for *n*-C33. The highest quantities occur in a marl. The average chain length (ACL) varies between 28 and 30.4, averaging around 29.4. Sharp excursions towards higher ACL values are found at 112.5 meter (5.396 Ma), 124.5 meter (5.389 Ma) and 237 meter (5.340 Ma). These excursions are all succeeded by an immediate decrease in ACL. The carbon preference index (CPI) fluctuates between 1.8 and 5.3, indicating an odd over even predominance. A large excursion towards a high CPI is found in cycle 5 at 112.5 meter (5.396 Ma), coinciding with the increase in ACL values, after which these values decrease sharply to 2.2 at the start of cycle 6. Cycle 6 is studied in a higher resolution (Figure 11) and changing CPI values between 1.7 and 4.7 are found, with again an increase to a CPI of 4.7 at 124.5 meter (5.3893 Ma), succeeded by a decrease of both CPI and ACL values at the start of the cycle (126 meter, 5.3889 Ma). After this decrease, CPI values increase while ACL values still decrease at 128.5 meter (5.3883 Ma). These values are succeeded by a decreasing trend in cycle 6 and lower amplitude variations in CPI values throughout the rest of the section. The ACL values remain relatively stable and show a small decrease towards the end of cycle 6 with also smaller fluctuations towards the end of the Upper Gypsum (the Miocene - Pliocene boundary). Overall, both CPI and ACL values show an increasing trend at the start of the section with higher amplitude variations and decreasing values towards the end of the section with lower amplitude variations (Fig 10 b,c, Figure 11 b,c). Samples from the Realmonte salt mine, consisting of kianite and alternating halite and clay laminae, also contain *n*-alkanes with CPI values of 2.2 and 3.4 and with constant ACL values of 29 and 29.1.

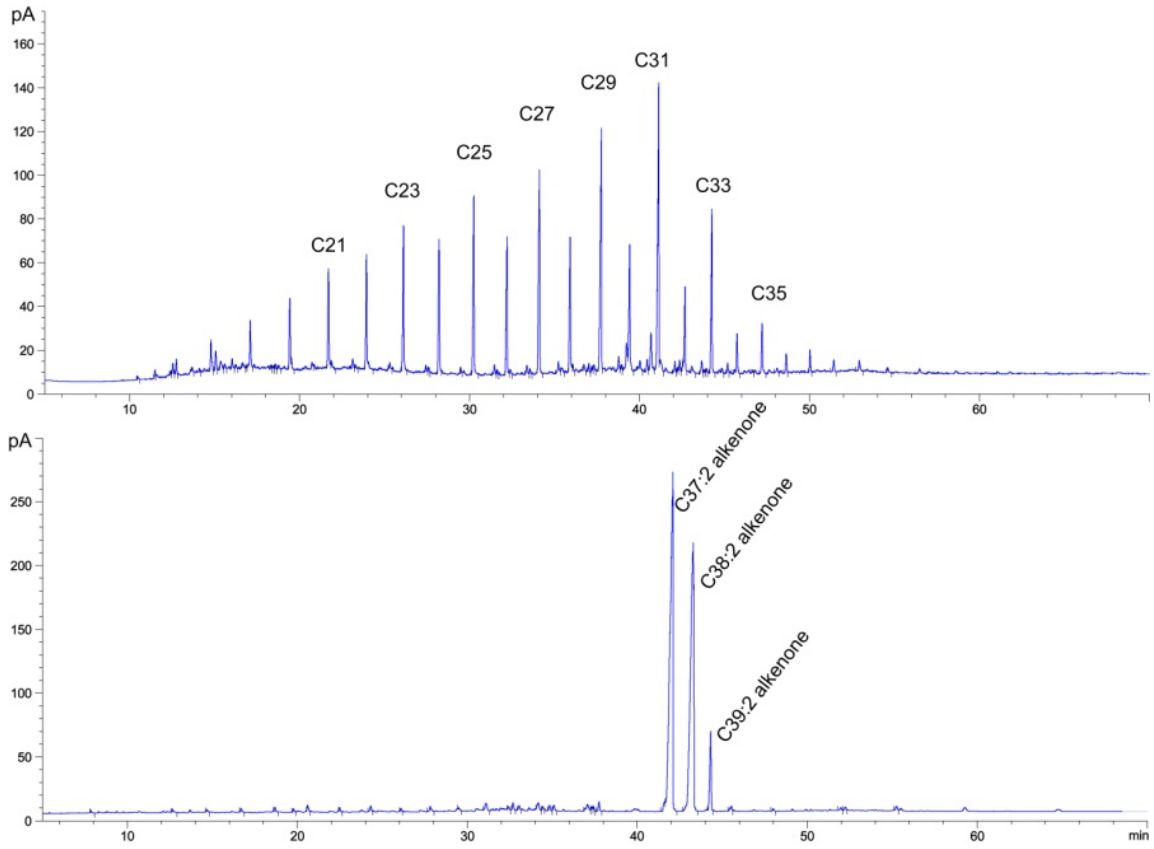

Figure 8 GC-FID (Flame Ionization Detector) chromatogram of the a-polar fraction (*n*-alkanes) and ketone fraction (C37:2, C38:2 and C39:2 alkenones) of an Eraclea Minoa sample (170 meter, ~5.38 Ma). The relatively early retention time of the ketones can be addressed to the fact that the in between these measurements, the column was trimmed.

4.3 Ketones

Well preserved long chain ketones are found from the second part of cycle 5 (112.5 meter, 5.396 Ma) onward. Cycle 6 was studied in a high resolution and an almost constant presence of these biomarkers

throughout the cycle is found. Quantities vary from 0.029 µg/g for the C37:2 ketone to 0.035 µg/g for the C38:2 ketone and 0.006 µg/g for the C39:2 ketones. In order to identify the structures of these ketones, a ketone sample was also measured on the GCxGC-TOF(MS). The samples mainly contain di-and tri-unsaturated C37 methyl ketones (C37:2 MK and C37:3 EK, M^+:530.543 and M^+: 528.527), di-unsaturated C38 methyl and ethyl ketones (C38:2 MK/EK, M^+: 544.563) and di-unsaturated C39 ethyl-ketones (C39:2 EK, M^+: 558.602). A strong co-elution of the C38:2 MK and EK is found, with a dominance of the C38:2 EK. $U^{k'}_{37}$ values vary between 0.72 and 0.95 with two sharp negative excursions at 118 meter (5.3910 Ma) and 238.2 meter (5.3387 Ma) and a small negative excursion at 124.5 meter (5.3893 Ma). Furthermore, ketones were also present in the salts of the Realmonte salt mine, which post-date the Lower Gypsum and pre-date the Upper Evaporites.

4.4 Hydrogen isotopes

A clear correlation pattern can be seen when comparing the δD values of the different long chain *n*-alkanes (C25-C31, Figure 9a). With a decreasing chain length, the hydrogen isotopic values become more deuterium enriched. The difference in δD values between the C25 and C31 *n*-alkanes varies up to 32.1‰. The standard deviations of the individual *n*-alkanes range from 0.8 to 3.7. Since the ACL averages around the C29 *n*-alkane, the C29 *n*-alkane is plotted downcore in the correlation figures (Figures 10 and 11). Because the *n*-C31 has the most data points, only this correlation with the *n*-C29 is shown. The regression line of the correlation between the *n*-C29 and the *n*-C31 shows a good correlation with an R^2 of 0.75 in Figure 9b.

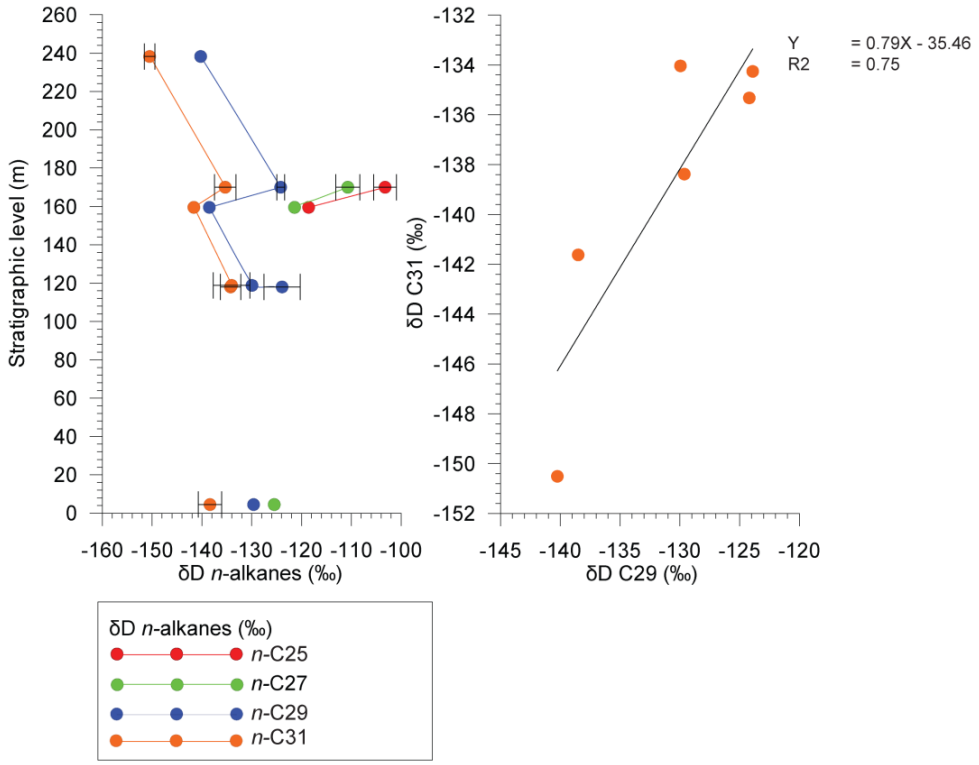

Figure 9 a) Compound specific δD values of the long chain *n*-alkanes C25-C31; b) correlation between the *n*-C29 and *n*-C31 alkane, including the regression line and R^2 value.

Compound specific hydrogen isotopic values of the C29 *n*-alkane range from -129.6‰ at the start of the section (4.5 meter, 5.4837 Ma) to deuterium enriched values of -123.9‰ at 118 meter (5.3910 Ma), after which the δD decreases again towards a value of -138.5‰ at 159.5 meter (5.3801 Ma). This decrease is succeeded by an increase in δD to -124.2‰ at 170 meter (5.3774 Ma), which is again followed by a decrease to -140.2‰ towards the end of the section (238.2 meter, 5.3387 Ma). The standard deviations range from 0.8 at 170 meter to 3.6 at 118 meter. When looking at this section in a smaller scale (cycle 6, Figure 11), a sharp decrease in hydrogen isotopic values can be observed at the start of cycle 6 (118.8 meter, 5.3908 Ma). This

decrease continues gradually up to approximately half of the cycle, after which the δD values increase again. Compound specific hydrogen isotopes have also been measures for the C17 and C33 *n*-alkanes and are shown in Table 1. The δD value of the *n*-C17 of -104.9‰ with a standard deviation of 3.98 (238.2 meter, 5.3387 Ma) is relatively much heavier than the δD of the long chain *n*-alkanes. The δD of the long chain *n*-C33 varies from -131.9‰ to -128.1‰, not following the general pattern of an increasing δD with a decreasing chain length.

The hydrogen isotopic values of the C37:2 Methyl and C38:2 Ethyl ketones show approximately the same overall trend throughout the section, with fluctuating C37:2 MK values from -165.1‰ to -203‰ and standard deviations from 3.2 to 3.3. The C38:2 EK δD values vary from -145.6‰ to -202.9‰ with standard deviations from 2.9 to 5.4 (Figure 10f, Table 2). A sharp decrease in δD can be found from the end of cycle 5 (112.5 meter, 5.3962 Ma), which is also the start of the presence of ketones, to the start of cycle 6 (126.5 meter, 5.3888 Ma). Succeeding, the δD again increases fast until 128.5 meter (5.3884 Ma) after which it continues its increasing trend towards 170 meter (5.3774 Ma) (Figure 10f). The δD values increase again towards the end of the section (238.2 meter, 5.3387 Ma). Remarkably, there is no clear pattern from shorter to longer chain ketones as it is found for the long chain *n*-alkanes based on hydrogen isotopes: C38:2 EK appears to have slightly higher values from 112.5 to 159.5 meter than C37:2 MK, while it is the other way around toward the end of the section. The C39:2 EK δD values were also measured, ranging from -169.8‰ to -166.7‰ (respectively at 159.5 and 170 meter, Table 2).

4.5 Lithology versus results

Hydrogen isotopic measurements for the *n*-alkanes are applied in marls and a banded selenite (facies A and C, Table 1, Figure 15). The banded selenite sample is located at the start of the section (4.5 meter) and does not show extremely different values compared to the rest of the δD values of the *n*-alkanes (Table 1, Figure 10d). For the ketones, hydrogen isotopes have been measured in selenite crust, gypsum cumulate and marls (facies A, B and C, Table 2, Figure 15). Interestingly, δD values of the selenite crust (respectively at 112.5 meter, 5.3962 Ma) are the most deuterium enriched (-145.6‰), while the banded selenites show the lowest hydrogen isotopic values (respectively -202.2‰ at 126.5 meter, 5.3888 Ma, Figure 10f). Furthermore, the selenite crust sample at 112.5 meter shows the most extreme CPI values of 11.17 and coincides with the first occurrence of the ketones in this section. For both evaporite samples, $U^{k'}_{37}$ values are high (>0.97). The Real Monte salt mine samples have a very low $U^{k'}_{37}$ value of 0.59 and a low CPI from 2.2 to 3.4.

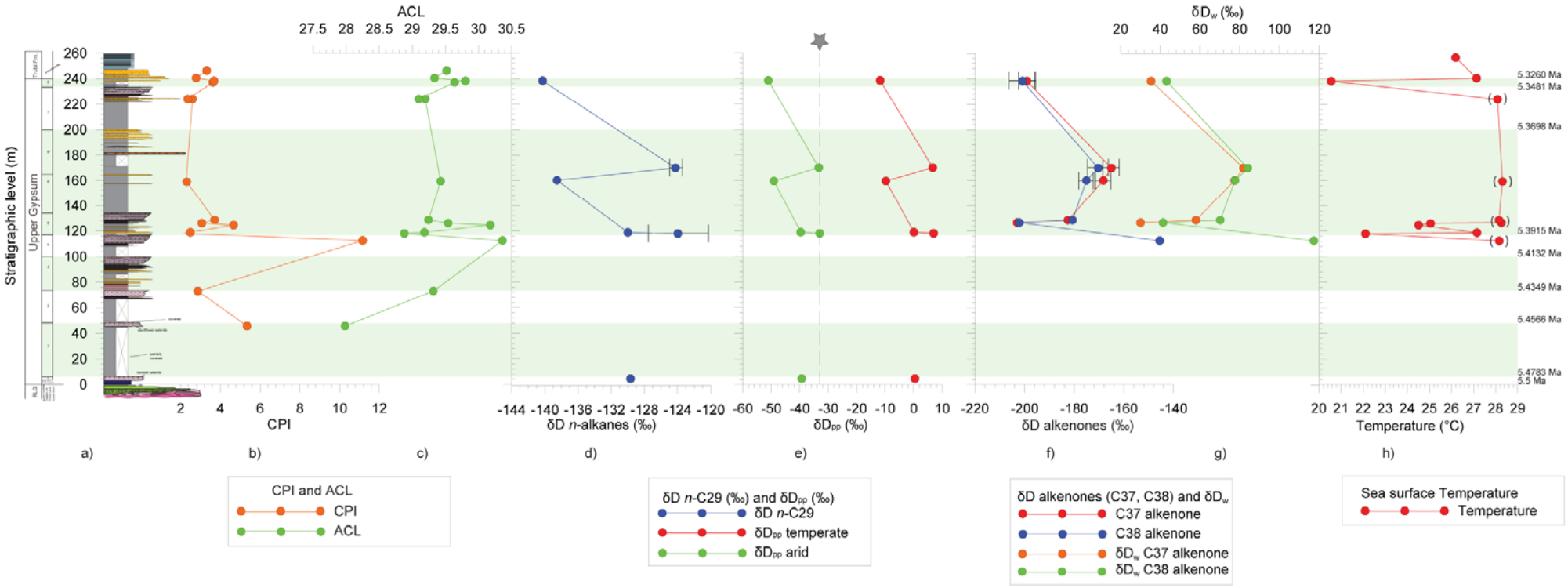

Figure 10 Results of the hydrogen isotopic (δD) measurements on terrestrial *n*-alkanes (C29 and C31) and ketones (C37:2 and C38:2), calculated hydrogen isotopic composition of the precipitation and the Eastern Mediterranean surface water and calculated CPI, ACL and temperature with: a) Schematic lithological column of Eraclea Minoa (Sicily), Italy; b) Carbon Preference Index (CPI) values of all *n*-alkanes; c) Average Chain Length (ACL) of all n-alkanes; d) Hydrogen isotopic values of long chain terrestrial *n*-alkane C29; e) Calculated precipitation values in a modern European climate with a fractionation of -130‰ (25) and in a desert climate with a net fractionation of -94‰ (26), the star with the dashed line indicates the present-day value (IAEA.org); f) Measured δD composition of ketones; g) δD of the Eastern Mediterranean surface water: the fractionation factors for the C37:2 MK and C38:2 EK ketones are respectively 0.732 and 0.745 and the enrichment factors are -225‰ and -233‰ (13); h) Sea Surface Temperatures, converted from the global core top calibration of the Uk'37 ratio (Uk'37 = 0.33*T + 0.44) (27). The highest SST are between brackets, because the upper limit of these values is determined by the method.

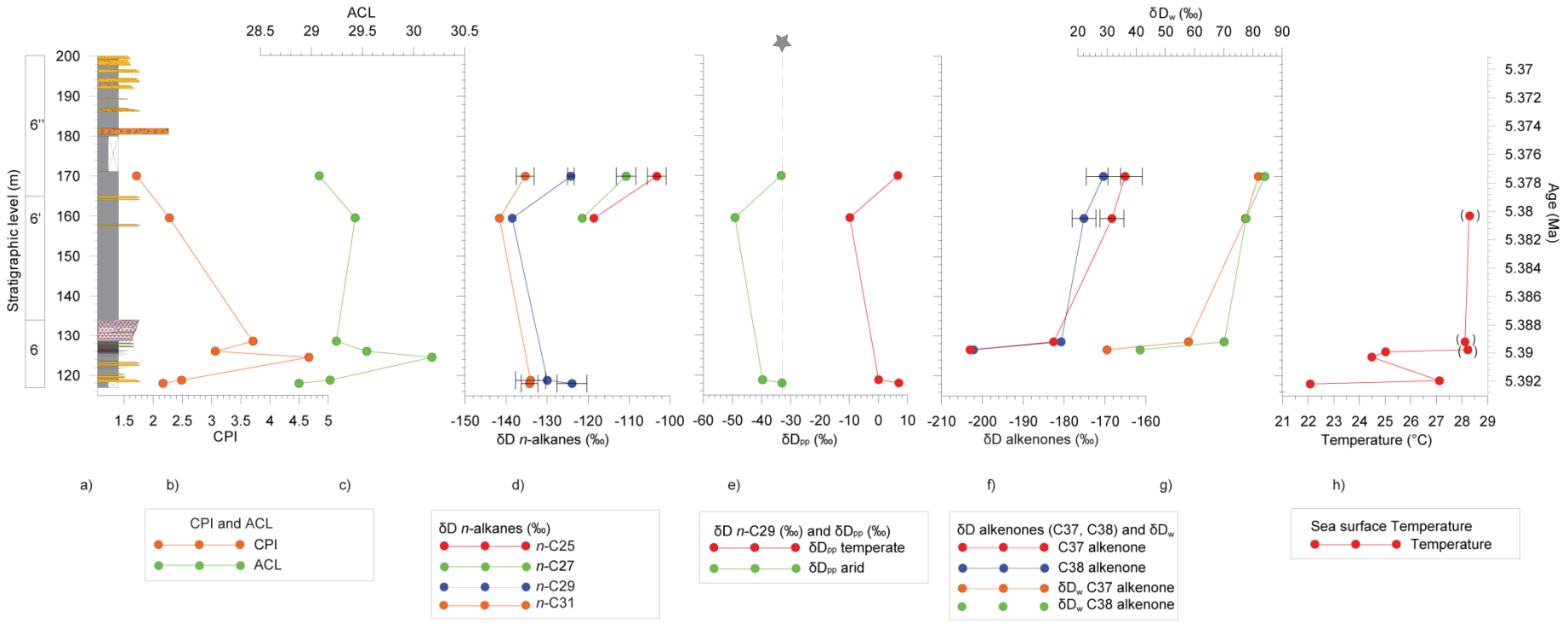

Figure 11 Results in a higher resoltution (cycle 6) of the hydrogen isotopic (δD) measurements on terrestrial *n*-alkanes (C29 and C31) and ketones (C37:2 and C38:2), calculated hydrogen isotopic composition of the precipitation and the Eastern Mediterranean surface water and calculated CPI, ACL and temperature with: a) Schematic lithological column of cycle 6 of Eraclea Minoa (Sicily), Italy;b) CPI ; c) ACL; d) Measured δD values of *n*-C25 to C31; e) Calculated precipitation values in a modern European climate with a fractionation of -130‰ (25) and in a desert climate with a net fractionation of -94‰ (26), the star with the dashed line indicates the present-day value (IAEA.org); f) Measured δD composition of ketones; g) δD of the Eastern Mediterranean surface water: the fractionation factors for the C37:2 MK and C38:2 EK ketones are respectively 0.732 and 0.745 and the enrichment factors are -225‰ and -233‰ (13); h) Sea Surface Temperatures, converted from the global core top calibration of the Uk'37 ratio (Uk'37 = 0.33*T + 0.44) (27). The highest SST are between brackets, because the upper limit of these values is determined by the method.

Strati-graphic level (m)	Age (Ma)	Sample	Lithology	Compo-nent	Amplitu-de (mV)	δD (‰)	δD mean (‰)	STD	δD_{water} (‰)	δD_{pp} tempe-rate (‰)	δD_{pp} dry (‰)
4.5	5.4837	EM-og15	banded selenite	C27	521	-125.5	-	-	-	5.2	-34.8
				C29	611	-129.6	-	-	-	0.4	-39.3
				C31	962	-140.1	-138.4	2.4	-	-9.6	-49.0
				C31	534	-136.7					
118	5.391	EM-og1	marl	C29	436	-126.5	-123.9	3.6	-	7.0	-33.0
				C29	404	-121.3					
				C31	504	-132.8	-134.3	2.1	-	-4.9	-44.4
				C31	411	-135.7					
118.8	5.3908	EM-og2	marl	C29	509	-130.0	-	-	-	0.1	-39.7
				C31	439	-131.4	-134.0	3.7	-	-4.6	-44.2
				C31	639	-136.6					
159.5	5.3801	EM-6[1]-26	marl	C25	458	-118.6	-	-	-	13.1	-27.1
				C27	693	-121.4	-	-	-	9.9	-30.2
				C29	1081	-138.5	-	-		-9.8	-49.1
				C31	1332	-141.6	-	-	-	-13.4	-52.6
				C33	649	-131.9	-	-	-	-2.2	-41.9
170	5.3774	EM-6[2]-7	marl	C21	402	-105.5	-	-	61.13		
				C23	552	-91.9	-	-	77.22		
				C25	619	-104.8	-103.2	2.3	-	30.8	-10.2
				C25	422	-101.6					
				C27	829	-111.1	-110.7	2.4	-	22.2	-18.4
				C27	565	-108.2					
				C27	786	-112.9					
				C29	962	-123.7	-124.2	0.8	-	6.7	-33.3
				C29	633	-123.8					
				C29	895	-125.1					
				C31	1149	-136.6	-135.3	2.2	-	-6.1	-45.6
				C31	773	-132.8					
				C31	1125	-136.6					
				C33	649	-129.4	-128.7	0.9	-	1.5	-38.3
				C33	600	-128.1					
238.2	5.3387	EM-8-6	marl	C17	499	-107.6	-104.9	3.8	61.8	-	-
				C17	820	-102.2					
				C29	473	-140.3	-	-	-	-11.8	-51.1
				C31	444	-149.8	-150.5	1.1	-	-23.6	-62.4
				C31	686	-151.3					

Table 1 Overview of the hydrogen isotopic values of the *n*-alkanes and associated calculated precipitation values in both temperate and dry conditions (25,26).

Strati-graphic level (m)	Age (Ma)	Sample	Lithology	Compo-nent	Amplitu-de (mV)	δD (‰)	δD mean (‰)	STD	δD_{water} (‰)
112.5	5.3962	EMRa	selenite crust	C38	416	-145.6	-	-	117.3
126.5	5.3888	EM-og9	gypsum cumulate	C37	470	-203.1	-	-	30.0
				C38	472	-202.2	-	-	41.3
128.5	5.3883	EM-og12	marl	C37	428	-182.6	-	-	57.9
				C38	434	-180.8	-	-	70.1
159.5	5.3801	EM-6"-26	marl	C37	3073	-168.1	-168.3	3.2	77.4
				C37	1524	-167.9			
				C37	1354	-164.8			
				C37	1532	-172.5			
				C38	3450	-172.9	-175.2	2.9	77.6
				C38	1471	-176.8			
				C38	1306	-172.6			
				C38	1457	-178.4			
				C39	900	-169.8	-	-	-
170	5.3774	EM-6"-7	marl	C37	3302	-164.4	-165.1	3.3	81.8
				C37	1899	-160.8			
				C37	2556	-167.0			
				C37	2401	-168.3			
				C38	3935	-165.7	-170.4	4.2	84.0
				C38	1794	-168.2			
				C38	2585	-172.9			
				C38	2448	-174.9			
				C39	1093	-164.7	-166.7	2.3	-
				C39	419	-166.8			
				C39	657	-165.6			
				C39	615	-170.0			
238.2	5.3387	EM-8-6	marl	C37	609	-197.8	-199.2	3.2	35.3
				C37	768	-202.8			
				C37	733	-196.9			
				C38	587	-194.6	-200.9	5.4	43.1
				C38	798	-203.7			
				C38	742	-204.3			

Table 2 Ketone hydrogen isotopic values and associated hydrogen isotopic composition of the Mediterranean surface water (20).

5. Discussion

5.1 *n*-Alkanes

5.1.1 Identification

n-Alkanes are produced by both aquatic and terrestrial organisms. Usually, the odd shorter chain *n*-alkanes (C17-C23) are of marine origin, while odd long chain *n*-alkanes (C25-C31) are derived from terrestrial higher plant leaf waxes (28,29,37). The terrestrial input of the long chain *n*-alkanes was determined from the CPI and ACL values. The odd over even predominance (CPI) of the samples from 1.8 to 5.3 combined with an average ACL of 29.4 suggests a terrestrial origin, although a part of these *n*-alkanes with relatively low CPI values indicates mixing with other (marine) sources as well. The short chain C17 *n*-alkane is considered an indicator for algal and photosynthetic bacterial input (49).

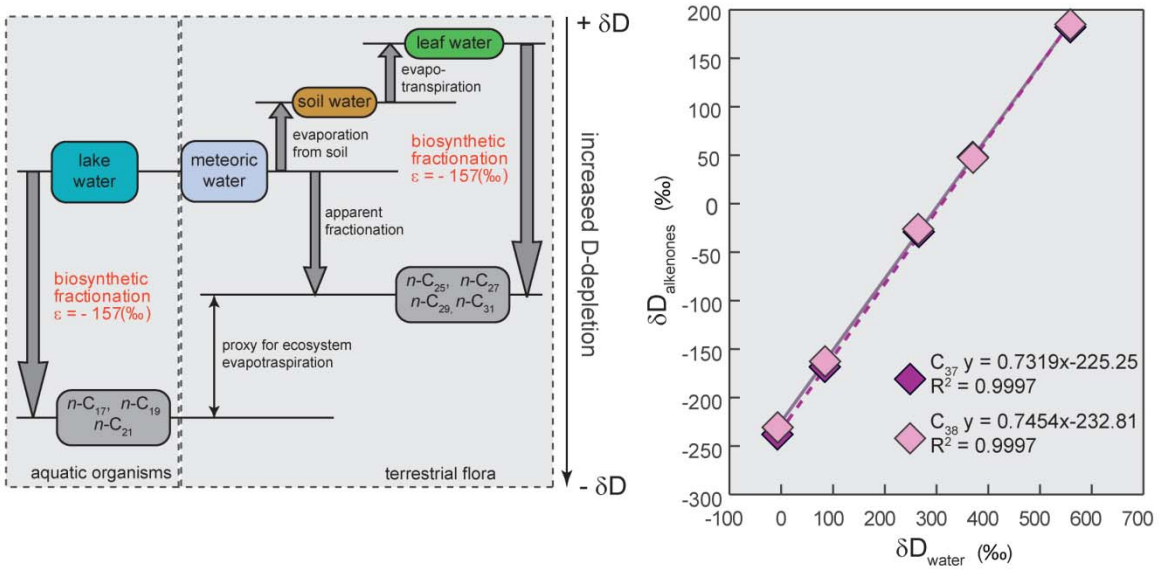

Figure 12 a) Schematic flow diagram of the fractionation between source water and aquatic and terrestrial *n*-alkanes, based on lake sediment sampling studies (modified after Sachse et al. 2006 (29)); b) Graph of the hydrogen isotopic composition of both C37 and C38 ketones from *Emiliania huxleyi* cultures in different deuterium enriched source waters (modified after Englebrecht and Sachs 2005 (13)).

5.1.2 Hydrogen isotopes

The distribution of hydrogen isotopes is closely related to the hydrological cycle and build-in organic molecules. The hydrogen isotopic composition of seawater can be recorded by the algal *n*-C17 alkane and mainly depends on the intensity of evaporation and influx of freshwater by rivers (27). When evaporation takes place, the residual water becomes increasingly enriched in deuterium (D). The long chain terrestrial *n*-alkanes (C25-C31) record the stable water isotopes in precipitation, which reflect the source region, water loss during transport, local temperature and the contribution of local water and mixing of air masses (21,24,25). In general, terrestrial *n*-alkanes are enriched in deuterium by 10 to 60‰ compared to aquatic *n*-alkanes due to leaf evaporation processes (Figure 12a) (29,37). This statement fits with our results, which shows a deuterium enrichment of maximum 44‰ between the long chain odd *n*-alkanes and *n*-C17 at 238.2 meter (5.3387 Ma). Based on a sampling study in recent lakes on a N-S European transect, the biosynthetic fractionation between the source water and the *n*-alkanes is considered to be constant around a mean of -157‰ for both aquatic and terrestrial *n*-alkanes (29,37). This value coincides with the biosynthetic fractionation factor found in laboratory experiments, which shows average fractionations between -158‰ and -162‰ dependant on the species (17).

Consequently, the source water hydrogen isotopic composition of the Mediterranean surface water can be calculated according to the following equations (37):

$$\varepsilon_{alkane/water} = 1000 * (\frac{\partial D_{alkane}+1000}{\partial D_{source\ water}+1000} - 1) \quad \text{(b)}$$

$$\partial D_{source\ water} = \frac{1000*(\partial D_{alkane} - \varepsilon_{alkane/water})}{\varepsilon_{alkane/water}+1000} \quad \text{(c)}$$

By inserting an average biosynthetic fractionation of -157‰ ($\varepsilon_{alkane/water}$), the resulting hydrogen isotopic value for the Mediterranean surface water based on the algal *n*-C17 is 61.80‰. This is heavy compared to present-day values of 8.40‰ in the Eastern Mediterranean summer (50). Furthermore, the hydrogen isotopic composition of the precipitation is calculated for two scenarios: a modern European (temperate) climate and a desert climate. The fractionation factor used determines the deuterium enrichment compared to δD of Sicily today (resp. ~-33.2‰, IAEA.org). As previously mentioned, the δD of terrestrial *n*-alkanes (C25–C31) mainly records the δD of precipitation, modified by meteorologic conditions (e.g. evapotranspiration in leaves) and plant anatomy (29). Based on the sampling study of Sachse et al. (2004), a fractionation of -130‰ is used for a modern European climate (37). The calculated deuterium enriched precipitation values during the Upper Evaporite deposition vary between -11.8‰ and +7.0‰ (Figure 10e, Table 1). Desert environments have a fractionation of -94‰, which is one of the smallest net fractionations recorded due to high leaf water deuterium enrichment in an arid environment (32). In this case, precipitation values vary between -51‰ and -31‰ (Figure 10e, Table 1). These values are comparable to the present-day hydrogen isotopic composition of precipitation in Sicily. Furthermore, calculated precipitation values could also be skewed somewhat to heavier (marine) values because of the relatively low CPI in some samples, indicating a low terrestrial input.

Summarized, the reconstructed δD of the precipitation is dependent on the fractionation factor used. These values are very high in a temperate climate setting, albeit that admixing from marine sources could have contributed to these heavy values as well. This could be the case for the start (118, 5.391 Ma) and the third sub-cycle of cycle 6 (170 meter, 5.3774 Ma), both containing the most deuterium enriched precipitation values (Table 1) and the lowest CPI values of 2.2 and 1.7 (Figure 10). These deuterium enriched values could be explained by extremely high evaporation rates of the Mediterranean, adding heavy isotopes to the precipitation. The calculated precipitation values in an arid climate are comparable to present-day values, which does not necessarily mean that evaporation rates were low. Possible explanations are that evaporation did take place, but was not extreme enough to evaporate the deuterium isotopes or that the evaporation was comparable to nowadays. A way to check these scenarios is by analyzing the hydrogen isotopic values of the Messinian Mediterranean surface waters, based on (comparisons between) hydrogen isotopic compositions of long chain ketones and the *n*-C17 alkane.

5.2 Ketones

5.2.1 Identification

In both recent and ancient sediments, long chain ketones with di- and tri-unsaturations (C37-C39 MK and EK) are found (40). The origin of the ketones found in Eraclea Minoa (respectively C37:2 MK, 38:2 EK and C39:2 EK) was determined by comparing these structures to present-day species. The cosmopolitan coccolithophorid *Emiliania huxleyi* is considered nowadays as a major producer of a range of C37-C39 MK and EK and is dominant in coastal waters as well as the open ocean (51). Because it is not known which haptophyte algae lived during the Miocene, the assumption was made that these species are a precursor of the species living nowadays (resp. *Emiliania huxleyi*). However, this is only based on similarities in molecular masses of the long chain alkenones and more research is needed to confirm this statement. Presence of ketones in the Upper

Evaporites suggests that the connections between Atlantic and Mediterranean, despite being reduced, were open also during stage 3 of the MSC. Also the absence of C37:4 ketones, an indicator of restricted lake environments, in the Eraclea Minoa section is characteristic for open marine settings (52). This statement contradicts the general opinion until now that connections between the Atlantic and Mediterranean were closed during deposition of the Upper Evaporites (14). Furthermore, the presence of ketones in the halite samples of the Real Monte salt mine, located between the Lower and Upper Evaporites, suggests that stratification of the water column during the ultimate brine level still enabled the haptophyte algae to survive.

5.2.2 Hydrogen isotopes

A culturing study, in which two species of haptophyte algae were cultured (*Emiliania huxleyi and Gephyrocapsa oceanica*) at different temperatures; salinities; and δD of the water, concluded that the δD of long chain alkenones mainly depends on the δD of the water, but also on salinity and to some degree growth rate (20). The δD of the seawater, in turn, mainly reflects salinity. The δD of the Eastern Mediterranean surface waters was calculated, according to the following equations (Figure 12b, (13)):

$$\partial \mathrm{D}_{\mathrm{C37:2}} = 0.7319 * \partial \mathrm{D}_{\mathrm{water}} - 225 \quad \text{(i)}$$

$$\partial \mathrm{D}_{\mathrm{C38:2}} = 0.7454 * \partial \mathrm{D}_{\mathrm{water}} - 233 \quad \text{(j)}$$

These formulas are based on another culturing study of the coccolithophorid *Emiliania Huxleyi*, which gave fractionation factors between the water and the ketone δD of 0.732 and 0.745 (13). The enrichment factors (ε) are respectively -225‰ and -233‰ (13). The calculated hydrogen isotopic composition of the Mediterranean surface water varies from 30‰ to an extreme of 117.31‰ in the selenite crust, averaging around a value of ~65.1‰ (Figure 10g, Table 2). These values are very heavy and in line with exceptional high rates of evaporation under extremely dry conditions. Equivalents of these values nowadays are only found in coastal sabkhas (δD<+30‰ (53)), deserts with a low humidity and desiccating ponds (δD<+100‰ (16,54)). The presence of primary gypsum deposits confirms these dry evaporative conditions, requiring a very high salinity of at least 130 g/l (11). The δD values obtained from the ketones are comparable to the Mediterranean hydrogen isotopic composition of 61.80‰ from the marine C17 *n*-alkane.

5.3 Environmental reconstruction

5.3.1 Sea Surface Temperatures

Sea surface temperatures (SST) were reconstructed by the alkenone unsaturation index ($U^{k'}_{37}$), monitoring the ratio between the di- and tri-unsaturated alkenones (17). The degree of unsaturation of C37 ketones is shown to be primarily a function of temperature in both core-top and culture experiments (40,55). SST values were converted from the global core top calibration of the $U^{k'}_{37}$ ratio, whereby the upper limit is determined by the method (i.e. $U^{k'}_{37}$ reaches its maximum value of 1 at ~28˚C (41)):

$$\mathrm{U}^{\mathrm{k}\prime}_{37} = 0.33 * \mathrm{T} + 0.044 \quad \text{(h)}$$

The warm SST varies between ~20.5˚C and ~28.3˚C, averaging around 26.1˚C (Figure 10h). This confirms the theory of warm temperature, under which a lot of evaporation can take place. However, as previously mentioned temperatures might be higher than the calculated values, since the method is only reliable for temperatures up to 28˚C.

5.3.2 Salinities

Because of the cyclic deposition of gypsum, it is assumed that salinities were varying but high. Modeling studies of Meijer and Krijgsman (2005) showed that gypsum precipitation during the MSC started after a sea level lowering of 2000 meters and required a (minimum) mean salinity of 130 g/l (11). The presence

of ketones suggests that connections with the Atlantic were still open and a stratification might have occurred with brine circumstances in the lower water column and less saline surface water. In culturing studies by Schouten et al. (2006), it is shown that also salinity variations have an impact on the fractionation during synthesis of alkenones. However, a sampling study by Schwab et al. (2011) to determine the relationship between hydrogen isotope ratios of individual ketones to sea water hydrogen isotopic values and salinity, showed no net change in alkenone-water D/H fractionation as a result of salinity increase (42). They came up with two probable explanations for this result: 1) the assembly of alkenone-producing haptophyte algae changes along the transect and have different sensitivities to salinity, which results in no apparent fractionation trend along a salinity gradient and; 2) a diminished sensitivity of alkenone-water hydrogen isotopic fractionation to salinity changes, due to greater osmoregulation capacity in coastal haptophytes (42). However, the high presence of the C37:4 in the sampling study of Schwab et al. (2011) indicates that these species differ sufficiently from the species found in our samples (with an absence of the C37:4 ketones) and other culturing studies also show that salinity influences the hydrogen isotope fractionation during lipid biosynthesis by algae (42,43,60). Since the mechanism is not resolved yet, the hydrogen isotopic composition of alkenones cannot be used to reconstruct paleosalinities directly. To be able to still have an indication of salinities in this study, the following hypothesis is proposed. Considering the Mediterranean as a closed system, precipitation is formed by the evaporation of the Mediterranean sea water and accumulates on land and in rivers, which (again) end up in the sea water. Precipitation is also taken up by the terrestrial vegetation, modified by biosynthesis and evapotranspiration, and seawater is used by the algae in the surface water for photosynthesis. Salinities are reconstructed based on the calculated δD of precipitation from the *n*-alkanes in dry and temperate conditions and the δD of the seawater from the ketones, with assumptions that the salinity of precipitation and the river input is 0 g/l and the global average δD of seawater is 0‰ with a salinity of 35 g/l. Based on this, a linear relation between salinity and δD is formed (Figure 13b,c). This linear relation is confirmed by present-day salinities and calculated δD values from the Mediterranean and Red Sea, which are plotted for comparison next to the MSC salinity reconstructions in a dry climate (Figure 13a).

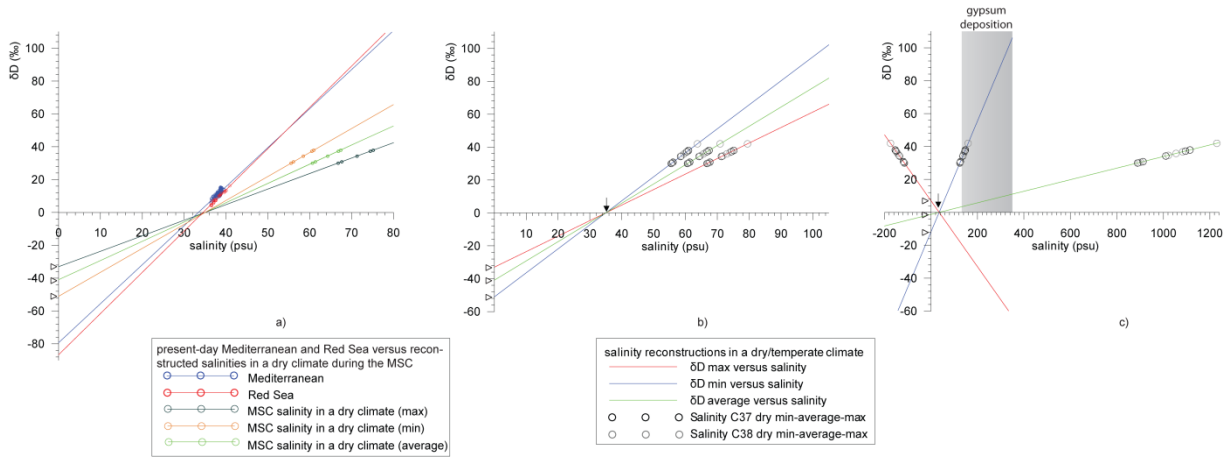

Figure 13 Reconstructed salinities in an arid and temperate climate, compared to present-day salinities of the Mediterranean and Red Sea with: a) calculated δD values (based on $\delta^{18}O$ measurements, multiplied by a factor 8) and measured salinities of the Mediterranean (30-45˚N, -6-36˚E, regression: δD = 2.3753s - 79.304 (56,57,58)) and Red Sea (12-29˚N, 32-43˚E, regression: δD = 2.5106s - 86.655 (59)), compared to reconstructed salinities during Upper Evaporite deposition based on calculated precipitation values in a dry climate (minimum, average and maximum: triangles) from the C29 *n*-alkane and the hydrogen isotopic composition of the seawater from C37 ketones; b) reconstructed salinities in a dry climate, based on the calculated Messinian precipitation values (minimum: -51.05‰, average: -40.92‰ and maximum: -33.01‰, triangles) of the C29 *n*-alkane, calculated δD of the seawater from the C37:2 and C38:2 ketones and with the assumption that the average salinity of seawater is 35 psu (≈ 35g/l) with δD=0 (arrow); c) reconstructed salinities in a temperate climate based on the calculated precipitation values (minimum: -51.05‰, average: -40.92‰ and maximum: -33.01‰, triangles) of the C29 *n*-alkane, calculated δD of the seawater from the C37:2 and C38:2 ketones and with the assumption that the average salinity of seawater is 35 psu with δD=0 (arrow).

The more negative δD values of the present-day Mediterranean and Red Sea at a salinity of 0 g/l (which can also be considered as the Mediterranean river input) can be explained by other and more river inputs nowadays with more deuterium depleted values. The reconstructed salinities in a temperate climate (Figure 13c) range from -154.2 to 1114 g/l for the C37 ketones and between -148.7 and 1083.2 g/l (≈ -148.7 and 1083.2 psu) for the C38 ketones. Since negative salinities do not exist and these extreme ranges cannot be used to reconstruct salinities, this could mean that the reconstruction of the δD of the precipitation in a temperate climate setting is not reliable for the MSC or that the model to reconstruct salinities is incorrect. However, it is more likely that the extreme high rates of evaporation needed for the precipitation of gypsum and the deuterium enriched surface water values occurred in a dry and warm climate. The reconstructed salinity in a dry climate setting varies from 55.5 to 75.2 g/l for the C37 ketones and from 55.2 to 79.5 g/l for the C38 ketones. Compared to an average present-day salinity of the Mediterranean of 38.45 g/l and average salinity of global seawater of 35 g/l, the calculated salinities are high but not extreme enough for gypsum precipitation starting at 130 g/l and 350 g/l (11,56,57,58). These values confirm the stratification theory, in which the upper water column is less saline than the lower water column with brine circumstances, enabling the haptophyte algae to survive.

5.3.3 Overall changes Eraclea Minoa: a new hypothesis

The very heavy surface water values are in line with exceptional high rates of evaporation. Still, the presence of long chain ketones and absence of the C37:4 ketone in the Upper Evaporites suggests that connections between the Atlantic and Mediterranean, despite being reduced, were also open during stage 3 of the MSC. The deuterium enriched precipitation values in a temperate climate setting could be the result of the more heavy hydrogen isotopes from the seawater, being reflected in local rain on the Mediterranean coast, albeit that admixing of organic matter contributed to the heavy values as well (Figure 14). The high average SST and very dry conditions might have contributed to this extreme evaporation. However, the presence of long chain ketones suggest a dilution of the Mediterranean surface water and a stratification of the water column. In the lower water column, salinities increase due to high evaporation rates in a warm and dry environment. The upper part of the water column might be less saline due to the inflow from the Atlantic and precipitation, diluting the saline surface water. This stratification could explain the formation of gypsum deposits in brine circumstances in the lower water column and survival of open ocean haptophyte algal species in the upper water column. The relatively normal δD of the precipitation in a dry climate setting and the reconstructed salinities averaging around 65 g/l also confirm the stratification theory, since a minimum salinity of 130 g/l is required for the formation of gypsum. Furthermore, it is more likely that the extreme high rates of evaporation needed for the precipitation of gypsum and the deuterium enriched surface water values occurred in a dry and warm climate.

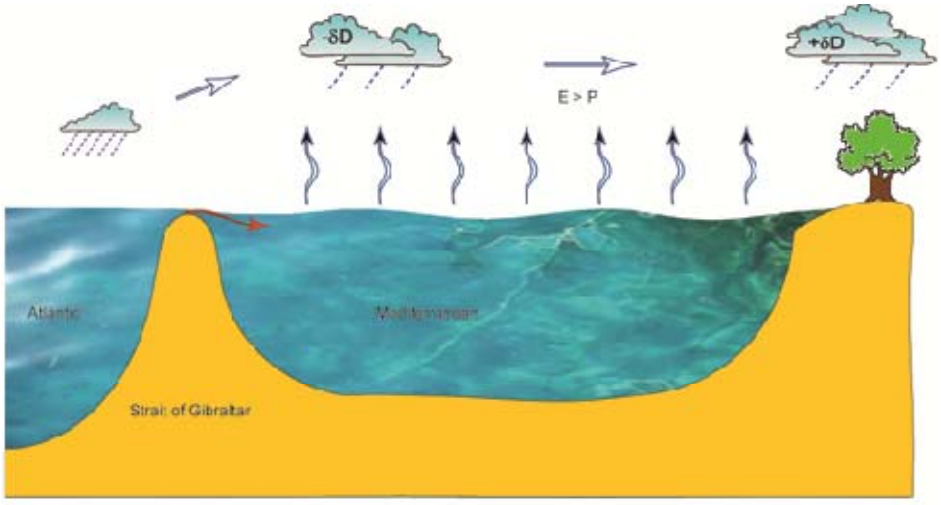

Figure 14 Our new hypothesis about the Messinian salinity crisis.

However, the proposed connection between the Atlantic and Mediterranean does not have to be continuous. In previous studies, paleontological and geochemical data also indicated that oceanic fluxes continued to enter the Mediterranean, with an increasing (fluvial) freshwater input through time (15). In the scenario of a non-continuous flow from the Atlantic into the Mediterranean, oceanic fluxes may have led to the inflow of coastal and open ocean algal species. After this inflow, an increased freshwater input causes stratification and dilution of the heavy saline surface waters in which these haptophyte algae can survive. This might also explain the sudden occurrence of these long chain ketones at the end of cycle 5, in which the increased freshwater input created favorable conditions for the survival of these species.

Until now, I have assumed that the precipitation of gypsum is only dependant on the salinity of the water column. In evaporative seawater, gypsum precipitated with 3 to 7 times concentrated ocean water (61). However, it should be taken into account that the equilibrium between dissolved calcium and sulphate is the primary control of gypsum precipitation (62).

5.3.4 Small scale changes (cycle 6)

In this study, cycle 6 was processed in a higher resolution to look at the changes in depositional environments within a cycle. In general, gypsum deposition is assumed to take place at insolation minima (arid climate), while dilution of the water column occurs at insolation maxima (1). For comparison, the facies interpretation of Manzi et al. (2009) is used, who also studied the Upper Evaporites of the Eraclea Minoa section (20). They subdivided the cycles into three facies associations (UGF, Figure 3), of which a short description will be given below (20).

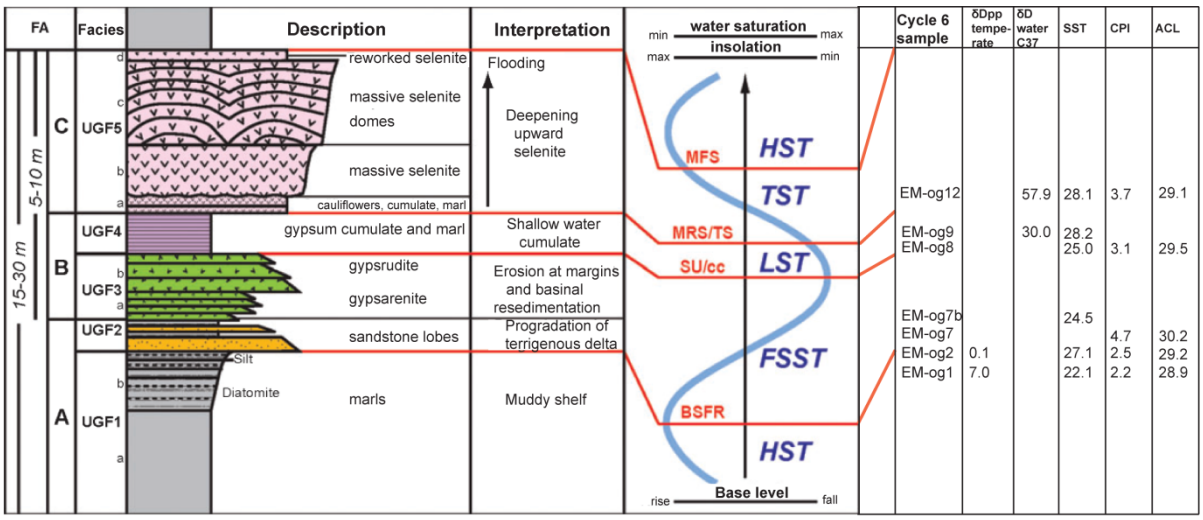

Figure 15 Ideal cycle for Upper Gypsum (modified after Schreiber 1997 and Manzi et al. (2009) (20)), including facies associations (A, B, C) and facies (UGF 1-5) and the results (calculated δD_{pp} in a temperate climate, δD_{water} from C37 ketones, SST, CPI and ACL) of the first sub-cycle of cycle 6 next to the corresponding facies.

The first part of a cycle (A), consisting of marl and sandstone packages, is interpreted as a shelf (marls) and prograding terrigenous deltaic system with moderate hypersaline to low salinity conditions (54). In our data, at the immediate start of cycle 6 (from 118 meter to 118.8 meter, UGF A), SST increase from 22.1˚C to 27.1˚C and CPI and ACL values increase slightly (Figures 11 and 15). Furthermore, the hydrogen isotopic composition of the precipitation in a temperate climate becomes more depleted from 7.0‰ to a value of 0.1‰ (respectively from -39.7‰ to -33‰ in a dry climate setting). This can be explained by the fact that UGF A is deposited during an insolation maximum, which is a period of a higher freshwater input that diluted the saline surface waters. This theory is also confirmed by the same transition from low to high SST, light δD values of the precipitation and the light δD of the ketones found in cycle 8, only consisting of UGF A (Figure 10). The CPI and ACL values also increase slightly during this time interval. The slight increase in CPI and ACL values indicates a change (but small) in composition of the vegetation, as well as a temporary higher terrestrial input. The second

part of a cycle (B) contains clastic gypsum beds (gypsarenite, gypsrudite and graded marl beds) and primary evaporitic laminar gypsum beds (gypsum cumulate). According to Manzi et al. (2009), the clastic gypsum beds are probably formed under gravity flows (erosion at margins and basinal resedimentation), confirmed by fallout sedimentary structures. The small crystals of the laminar gypsum beds are formed at the air-water interface in shallow water conditions, after which they settled to the bottom (54). The massive selenites of the third part of a cycle (C) start with relatively shallow water conditions and are assumed to indicate a deepening upward of the water column (Figure 15, (20)). From UGF A of the first sub-cycle of cycle 6 to UGF B, SST again decrease to 24.5˚C, after which it again increases (28.2˚C) towards the end of UGF B and the start of UGF C. Throughout the rest of cycle 6, consisting of UGF C succeeded by only UGF A for the last two sub-cycles, the SST are relatively stable but high. Based only on the reconstructed SST, this pattern appears to agree with the insolation pattern and interpretation of Manzi et al. (2006). However, more hydrogen isotopic measurements are needed to confirm this theory. From 118.8 meter (UGF A) to the second part of cycle 6 (UGF A, 159.5 meter, 5.3801 Ma), the δD of the precipitation decreases to -9.8‰ while CPI values decrease, the ACL value stays relatively stable with a slight increase. The gypsum cumulate of UGF B (126.5 meter, 5.3888 Ma) shows relatively light hydrogen isotopic values of the water column (~30‰), compared to the δD of the UGF C (57.90‰, 128.5 meter, 5.3883 Ma) and also CPI values increase slightly, while the ACL decreases. After this, the hydrogen isotopic composition of the Mediterranean shows a trend towards deuterium enriched values in the UGF A of the second sub-cycle (77.43, 159.5 meter, 5.3801 Ma) and UGF A of the third sub-cycle (81.84‰, 170 meter, 5.3774 Ma). Based on cycle 6, an increasing deuterium enrichment of the Mediterranean surface water is found from UGF B to UGF C. Furthermore, UGF B shows low SST that increase towards the start of UGF C, after which SST remain relatively stable. The deuterium enrichment from UGF B to C could be explained by an increase in evaporative conditions with a climax at the start of UGF C (maximum dryness, insolation minimum, increasing SST). Again, these values correlate with the theory proposed by Manzi et al. (2009), showing an insolation minimum at the end of UGF B (gypsum cumulate, low SST), with a small increase in insolation towards the start of UGF C (higher SST). For comparison, the first occurrence of long chain ketones in this section at the end of cycle 5 (UGF C, 112.5 meter, 5.3962 Ma) coincides with an extremely high CPI of 11.17, an ACL of 30.36, a high SST of 28.13 and also very deuterium enriched hydrogen isotopic values for the Mediterranean. Summarized, overall SST are high to enable high evaporation rates, with the lowest values at the start of UGF A and (the end of) UGF B. The highest SST are found in UGF C and after the middle of UGF A, coinciding with the insolation patterns described by Manzi et al. (2009). No clear pattern can be observed for the fluctuating CPI and ACL values, although slight small scale increases in CPI values (which are still low) appear to coincide with an increased freshwater input during insolation maxima. More hydrogen isotopic measurements are needed to find a conclusive relation between the data and hydrogen isotopic values, even though a light δD appears to coincide with an insolation maximum (humid conditions) in UGFB and deuterium enriched values coincide with high SST during the return from an insolation minimum to an insolation maximum in UGF C. Other factors that need to be incorporated are the (small) global sea level rise during this period and the (associated?) inflow from the Atlantic, leading to the inflow of the haptophyte algae. The first occurrence of these species, however, can be seen in a selenite crust of UGF C and coincides with very heavy surface water values of 117.3‰ from the C38 ketones. These heavy surface water values do not indicate dilution of the surface water by Atlantic inflow. However, more hydrogen isotopic data and a more detailed description of every cycle is needed to be able to explain these patterns.

6. Conclusions

The Upper Evaporites (5.50-5.33 Ma) were sampled from the Eraclea Minoa section (Sicily), in order to reconstruct hydrological changes during the Messinian Salinity Crisis, based on compound specific hydrogen isotopic measurements. Both long chain *n*-alkanes with an odd over even predominance (higher plants), as well as short chain aquatic *n*-C17 and long chain ketones are found, recording heavy (deuterium enriched) hydrogen isotopic values. The very heavy surface water values are in line with exceptional high rates of evaporation. The reconstructed δD of the precipitation is dependent on the fractionation factor used. The deuterium enriched precipitation values in a temperate climate setting could be a result of the more heavy hydrogen isotopes from the seawater being reflected in local rain on the Mediterranean coast, albeit that admixing of marine organic matter contributed to the heavy values as well. The calculated high SST and very dry conditions could have contributed to this high evaporation. However, the hydrogen isotopic composition of precipitation in a dry climate setting are comparable to present-day values and salinities average around 65 g/l, while gypsum deposition requires a salinity of 130 g/l. Furthermore, presence of long chain alkenones in the Upper Evaporites suggests a stratification of the water column and that the connections between Atlantic and Mediterranean, despite being reduced, were open during stage 3 of the MSC. Overall, high SST appear to coincide with the deposition of marls and sandstones at the start of the cycle and massive gypsum in the upper part of the cycles. However, hydrogen isotopic values are most deuterium enriched in the massive gypsum deposits where most evaporation takes place during an insolation minimum, while the most depleted values occur in the marls at the start of the cycle coinciding with an insolation maximum and a high freshwater input. More measurements are needed to study these changes in hydrogen isotopic values and their relation to climatic changes in detail.

7. Acknowledgements

First, I would like to thank my supervisors Gert-Jan Reichart and Iuliana Vasiliev for the opportunity to work on this nice subject and their great help, support, discussions and the opportunity to present my research at the EGU. Also thanks to Linda van Roij for her help in the laboratory. Furthermore, I would like to thank Johan Weijers and Els Soelen for their help and willingness to answer questions. Also special thanks to Stefano Lugli, Vinicio Manzi and Marco Roveri for the help (for Iuliana) with sampling of the section.

References

1) Krijgsman, W., Hilgen, F.J., Raffi, I., Sierro, F.J., Wilson, D.S. (1999), *Chronology, causes and progression of the Messinian salinity crisis*, Nature 400
2) Hsü, K.J., Ryan, W. B.F., Cita, M.B. (1973), *Late Miocene dessication of the Mediterranean*, Nature 242, 240-244
3) Hilgen, F.J., Krijgsman, W., Langereis, C.G., Lourens, L.J., Santarelli, A., Zachariasse, W.J. (1995), *Extending the astronomical (polarity) timescale into the Miocene*, Earth planet Scientific Letters, 136, 395-510
4) Krijgsman, W., Meijer, P. Th. (2008), *Depositional environments of the Mediterranean "Lower Evaporites" of the Messinian salinity crisis: Constraints from quantitative analysis*, Marine Geology 253, 73-81
5) Wijermans, R. (1988), *Neogene tectonics in the Western Mediterranean may have caused the Messinian Salinity Crisis and an associated glacial even*t, Tectonophysics 148, 211-219
6) Hodell, d. et al. (1994), *Magnetostratigraphic, biostratigraphic, and stable isotopic stratigraphy of an Upper Miocene drill core from the Salé Briqueterie (northwest Morocco): a high resolution chronology for the Messinian stage*, Paleoceanography 9, 835-855
7) Duggen, S., Hoernle, K., Van den Bogaard, P., Rupke, L. and Phipps Morgan, J. (2003), *Deep roots of the Messinian salinity crisis*, Nature 422, 602-607
8) Franseen, E.K., Goldstein, R.H. and Farr, M.R. (1998), *Quantitative controls on location and architecture of carbonate depositional sequences: upper Miocene, Cabo de Gata SE Spain*, Journal of Sedimentary Research 68, 283– 298
9) Roep, T.B., Dabrio, C.J., Fortuin, A.R., and Polo, M.D.(1998), *Late highstand patterns of shifting and stepping coastal barriers and shoverfans (late Messinian, Sorbas basin, SE Spain)*, Sedimentary Geology 116 27– 56.
10) Hodell, D.A., Curtis, J.H., Sierro, F.J., Raymo, M.E. (2001), *Correlation of Late Miocene to Early Pliocene sequences between the Mediterranean and North Atlantic*, Paleoceanography 16,164–178.
11) Meijer, P.Th. and Krijgsman, W. (2005), *A quantitative analysis of the desiccation and re-filling of the Mediterranean during the Messinian Salinity Crisis*, Earth and Planetary Science Letters 240, 510–520
12) Rouchy, J.M. and Caruso, A. (2006), *The Messinian salinity crisis in the Mediterranean basin: A reassessment of the data and an integrated scenario*, Sedimentary Geology 188-189, 35-67
13) Englebrecht, A.C. and Sachs, J.P. (2005), *Determination of sediment provenance at drift sites using hydrogen isotopes and unsaturation ratios in alkenones*, Geochimica et Cosmochimica Acta, Vol. 69, No. 17, pp. 4253-4265
14) Roveri, m., Manzi, V., Gennari, R., Iaccarino, S.M., Lugli, S. (2008), *Recent advancements in the Messinian stratigraphy of Italy and their Mediterranean-scale implications*, Bolletino della Societa Paleontologica Italiana, 47 (2), 71-85
15) Cita, M.B., Wright, R.C., Ryan, W.B.F. and Longinelli, A. (1978), *Messinian paleoenvironments, Initial Reports of the Deep Sea Drilling Project*, 42A, U.S. Government Printing Office, Washington, DC, pp. 1003–1035.
16) Andersen, N., Paul, H.A., Bernasconi, S.M., McKenzie, J.A., Behrends, A., Schaeffer, P., Albrecht, P. (2001), *Large and rapid climate variability during the Messinian salinity crisis: Evidence from deuterium concentrations of individual biomarkers,* Geology Vol. 29, 799-802
17) Sessions, A.L., Burgoye, T.W., Schimmelman, A., Hayes, J.M. (1999), *Fractionation of hydrogen isotopes in lipid biosynthesis*, Organic Geochemistry, v. 30, p. 1193-1200
18) Sessions, A.L., Sylva, S.P., Summons, R.E., Hayes, J.M., 2004. *Isotopic exchange of carbon-bound hydrogen over geologic timescales*. Geochimica et Cosmochima Acta 68, 1545–1559
19) Decima, A., Schreiber, B.C. and Mc Kenzie, J.A. (1988), *The origin of "evaporative" limestones: an example from the Messinian of Sicily (Italy)*, Journal of Sedimentary Petrology 58, 256-272

20) De Lange, G.J. and Manzi, V., Lugli, S., Roveri, M. and Charlotte, B. (2009), *A new facies model for the Upper Gypsum of Sicily (Italy): chronological and palaeoenvironmental constraints for the Messinian salinity crisis in the Mediterranean*, Sedimentology 56, 1937-1960
21) Speelman, E.N., J.O. Sewall, Noone, D., Huber, M., Von der Heydt, A., Damsté, J.S.S., Reichart, G.J. (2010), *Modelling the influence of a reduced equator-to-pole sea surface temperature gradient on the distribution of water isotopes in the Early/Middle Eocene*, Earth and Planetary Science Letters 298, 57-65
22) Sachse, D., Billault, I., Bowen, G.J., Chikaraishi, Y., Dawson, T.E., Feakins, S.J., Freeman, K.H., Magill, C.R., McInerney, F.A., Van der Meer, M.T.J., Polissar, P., Robins, R.J., Sachs, J.P., Schmidt, H.L., Sessions, A.L., White, J.W.C., West, J.B. and Kahmen, A. (2012), *Molecular Paleohydrology: Interpreting the Hydrogen-Isotopic composition of Lipid Biomarkers from Photosynthesizing Organisms*, Annual Reviews Earth Planetary Sciences 40, 221-49
23) Dansgaard, W. (1964), *Stable isotopes in precipitation*, Tellus 16, 436–68
24) Craig, H., Gordon, L.I. (1965), *Deuterium and oxygen 18 variations in the ocean and the marine atmosphere*, In: Tongiorgi, E. (Ed.), Stable isotopes in oceanographic studies and paleotemperatures. Lab. di Geol. Nucl, Pisa, Italy, 9–130
25) Merlivat, L., Jouzel, J. (1979), *Global climatic interpretation of the deuterium-oxygen 18 relationship for precipitation*, Journal Geophysical Research 84, 5029–5033
26) Dawson, T.E., Pate, J.S. (1996), *Seasonal water uptake and movement in root systems of Australian phraeatophytic plants of dimorphic root morphology: a stable isotope investigation*, Oecologia 107, 13–20
27) Schouten, S., Ossebaar, J., Schreiber, K., Kienhuis, M.V.M., Langer, G., Benthien, A., Bijma, J. (2006), *The effect of temperature, salinity and growth rate on the stable hydrogen isotopes of long chain alkenones, produced by Emilia huxleyi and Gephyrocapsa oceanic*, Biogeosciences, Vol. 3, pp. 113-119
28) Eglinton, G. and Hamilton, R.J. (1967), *Leaf epicutilar waxes*, Science 156, 1322-1334
29) Sachse, D., Radke, J., Gleixner, G. (2006*), dD values of individual n-alkanes from terrestrial plants along a climatic gradient – Implications for the sedimentary biomarker record*, Organic Geochemistry 37, 469-483
30) Smith, F.A., Freeman, K.H. (2006), *Influence of physiology and climate on δD of leaf wax n-alkanes from C3 and C4 grasses*, Geochimica et cosmochimica Acta 70, 1172-87
31) Schimmelmann, A., Lewan, M.D., Wintsch, R.P. (1999), *D/H isotope ratios of kerogen, bitumen, oil, and water in hydrous pyrolysis of source rocks containing kerogen types I, II, and III*, Geochimica et Cosmochimica Acta 63, 3751–3766
32) Feakins, S.J., Sessions, A.L. (2010), *Controls on the D/H ratios of plant leaf waxes in arid ecosystems*, Geochimica et Cosmochimica Acta, Vol. 74, pp. 2128-2141
33) Baas, M., Pancost, R., van Geel, B., Damste, J.S.S. (2000), *A comparative study of lipids in sphagnum species*, Organic Geochemistry 31 (6), 535–541
34) Sachse, D., Radke, J., Gleixner, G. (2004b), *Hydrogen isotope ratios of recent lacustrine sedimentary n-alkanes record modern climate variabilit*y. Geochimica et Cosmochima Acta 68, 4877–89
35) Hou, J.Z., D'Andrea, W.J., Huang, Y.S. (2008), *Can sedimentary leaf waxes record D/H ratios of continental precipitation? Field, model, and experimental assessments*, Geochimica et Cosmochimica Acta 72, 3503–17
36) Pedentchouk, N., Sumner, W., Tipple, B., Pagani, M. (2008), *δ13C and δD compositions of n-alkanes from modern angiosperms and conifers: an experimental setup in central Washington State, USA,* Organic Geochemistry 39, 1066–71
37) Sachse, D., Radke, J., Gleixner, G. (2004), *Hydrogen isotope ratios of recent lacustrine sedimentary n-alkanes record modern climate variability*, Geochimica et Cosmochimica Acta, Vol. 68, No. 23, pp. 4877–4889, 2004
38) Wolhowe, M. D., Prahl, F. G., Probert, I., Maldonado, M. (2009), *Growth phase dependent hydrogen isotopic fractionation in alkenone-producing haptophytes,* Biogeosciences 6, 1681–1694

39) Herbert, T. D. (2003), *Alkenone Paleotemperature Determinations*, Geochemistry 6, edited by: Turekian, K. K. and Holland, H. D., Elsevier, Oxford UK, 391–432
40) Prahl, F.G., Wakeham, S.G. (1987), *Calibration of unsaturation patterns in long-chain ketone compositions for paleotemperature assessment*, Letters to Nature vol. 220
41) Müller, P.J., Kirst, G., Ruhland, G., Von Storch, I., Rosell-Méle, A. (1998), *Calibration of the alkenone paleotemperature index Uk'37 based on core tops from the eastern South Atlantic and the global ocean (60˚N-60˚S*), Geochimica et Cosmochimica Acta, Vol. 62, No. 10, pp. 1757–1772
42) Schwab, V.F. and Sachs, J.P. (2011*), Hydrogen isotopes in individual alkenones from the Chesapake Bay estuary*, Geochimica et Geocosmica Acta 75, 7552-7565
43) Sachse, D. and Sachs, J. (2008), *Inverse relationship between D/H fractionation in cyanobacterial lipids and salinity in Christmas Island saline ponds*, Geochimica et Cosmochima Acta 72, 793–806.
44) Paul, H. (2002), *Application of novel stable isotope methods to reconstruct paleoenvironments, Compound specific hydrogen isotopes and pore-water oxygen isotopes*, PhD thesis, Swiss Federal Institute of Technology, pp. 149
45) Sessions, A.L., Hayes, J.M. (2005), *Calculation of hydrogen isotopic fractionations in biogeochemical systems*, Geochimica et Geocosmica Acta 69: No3, 593-597
46) Sternberg L. d. S. L. (1988), *D/H ratios of environmental water recorded by D/H ratios of plant lipids*, Nature 333, 59–61
47) Sauer, P. E., Eglinton, T. I., Hayes, J. M., Schimmelmann, A., Sessions, A. L. (2001), *Compound-specific D/H ratios of lipid biomarkers from sediments as a proxy for environmental and climatic conditions*, Geochimica et Cosmochimica Acta 65 (2), 213–222
48) Huang, Y., Shuman, B., Wang, Y., and Webb, T. I. (2002), *Hydrogen isotope ratios of palmitic acid in lacustrine sediments record late Quaternary climate variations*, Geology 30 (12), 1103–110
49) Han, J. and Calvin, M. (1969), *Hydrocarbon distribution of algae and bacteria and microbiological activity in sediments*, Proceedings of the National Academy of the United States of America 64, 29-33
50) Gat, J.R., Shemesh, A., Tziperman, E., Hecht, A., Georgopoulos, D., Basturk, O. (1996), *The stable isotopic composition of the eastern Mediterranean Sea, Journal of Geophysical research*, Vol. 101, No. C3, pp. 6441-6451
51) Volkman, J.K., Eglinton, G., Corner, E.D.S. and Sargent, J.R. (1980), *Novel unsaturated straight-chain methyl and ethyl ketones in marine sediments and a coccolithophore Emilia huxleyi*, Advances in Organic Geochemistry, pp219-227
52) Liu, W., Liu, Z., Wang, H., He, Y., Wang, Z., Xu, L. (2011), *Salinity control on long-chain alkenone distributions in lake surface waters and sediments of the northern Qinghai-Tibetan Plateau, China*, Geochimica et Cosmochimica Acta 75, 1693-1703
53) Gat, J.R., and Levy, Y. (1978), *Isotope hydrology of inland sabkhas in the Bardawil area*, Sinai: Limnology and Oceanography 23 841–850
54) Fontes, J.-C., and Gonfiantini, R. (1967), *Comportement isotopique au cours de l'évaporation de deux bassins sahariens*, Earth and Planetary Science Letters 3, 258–266, 386
55) Toney, J.L., Huang, Y., Fritz, S.C., Baker, P.A., Grimm, E., Nyren, P. (2010), *Climatic and environmental controls on the occurrence and distributions of long chain alkenones in lakes of the interior* United States Geochimica et Cosmochimica Acta 74, 1563–1578
56) Pierre, C., Vergnaud-Grazzini, C., Thouron, D., Saliege, J.F. (1986). *Compositions isotopiques de oxygène et du carbone des masses d'eau en Méditerranée*, Memorie Società Geologica Italiana 36, 165–174
57) Pierre, C. (1999), *The oxygen and carbon isotope distribution in the Mediterranean water masses*, Marine Geology 153, 41-55
58) Stahl, W., Rinow, U. (1973), *Sauerstoffisotopenanalysen an Mittelmeerwässern. Ein Beitrag zur Problematik von paläotemperaturbestimmungen*, "Meteor" Forschungsergebnis Reihe C 14, 55-59
59) Delaygue G., J. Jouzel, Dutay, J.-C (2000), *Salinity-oxygen 18 relationship simulated by an oceanic general circulation model*, Earth and Planetary Science Letters 178 (1-2), 118-138

60) Sachs, J. P. and Schwab, V. F. (2011), *Hydrogen isotopes in dinosterol from the Chesapeake Bay estuary*, Geochimica Cosmochimica Acta 72, 444–459.
61) De Lange, G.J., Boelrijk, N.A.I.M., Catalano, G., Corselli, C., Klinkhammer, G.P., Middelburg, J.J., Muller, D.W., Ullman, W.J., Van Gaans, P., Woittiez, J.R.W. (1990), *Sulphate-related equilibria in the hypersaline brines of the Tyro and Bannock Basins, eastern Mediterranean*, Marine Chemistry 31, 89–112.
62) Krijgsman, W. (2010), *Messinian salinity crisis: A novel unifying shallow gypsum/deep dolomite formation mechanism*, Marine Geology 275, 273-277